Electronic Supplementary Material (ESI) for New Journal of Chemistry.

Supporting Information

HF-Addition to Haloacetyl Fluorides in Superacidic Media

Sebastian Steiner,* Zurwa M. Shafiq, Alexander Nitzer, Dirk Hollenwäger and Andreas J. Kornath

Abstract: The reactions of difluoroacetyl fluoride and trifluoroacetyl fluoride were investigated in the binary superacid HF/SbF_5 by low-temperature NMR spectroscopy. Whereas both haloacetyl fluorides form oxonium species after the addition of HF, the protonated acyl fluorides were not observed. Protonated 1,1,2,2-tetrafluoroethanol was isolated as a solid and represents an example of a protonated α-fluoroalcohol. The salt was characterized by low-temperature vibrational spectroscopy and single-crystal X-ray diffraction. $[CHF_2CF_2OH_2][SbF_6]$ crystallizes in the triclinic space group $P\bar{1}$ with two formula units per unit cell. Protonated perfluoroethanol is only stable in solution. The reactivity of both haloacyl fluorides is discussed based on quantum chemical calculations at the MP2/aug-cc-pVTZ-level of theory.

Figures:

Tables:

Experimental Section

Caution! Avoid skin contact with all compounds. Hydrolysis can lead to the formation of HF or DF that burns skin and causes irreparable damage. Ensure appropriate safety precautions while handling these materials.

Apparatus and Materials: All reactions were performed employing standard Schlenk techniques using a stainless-steel vacuum line. Syntheses were carried out using FEP/PFA tube reactors closed with stainless-steel valves. Before use, the stainless-steel vacuum line and all reactors were dried with fluorine. Low-temperature Raman spectra were recorded under vacuum using glass cells cooled with liquid nitrogen and a Bruker® MultiRAMII FT Raman spectrometer equipped with Nd:YAG laser (λ = 1064 nm) and a laser excitation of 500-1000 mW. Low-temperature IR spectra were recorded with a Bruker® Vertex FT IR spectrometer at −196 °C. For measurements, low-temperature IR cells[1] were prepared with CsBr single-crystal plates coated with a small amount of the samples. For visualization, the software Advanced Chemistry Development Inc.® (ACD/Labs 2015) was employed. Low-temperature X-ray diffraction was performed with an Oxford XCalibur3 diffractometer equipped with a Spellman Generator (50 kV, 40 mA) and a Kappa CCD detector, using Mo-Kα radiation (λ = 0.71073 Å). The program CrysAlisPro 1.171.40.82a (Rigaku OD, 2020)[2] was employed for the data collection and reduction. The structure solution and refinement were performed with the software SHELXT[3] and SHELXL-2018/3,[4] implemented in the WinGX software package.[5] The solution was checked with the program PLATON[6] and the absorption correction was performed using the SCALE3 ABSPACK multi-scan-method.[7] Selected data and parameters of the single-crystal X-ray structure analyses are summarized in Table S4 for **1** (see Supporting Information). Crystallographic data (excluding structure factors) for the structures in this paper were deposited at the Cambridge Crystallographic Data Centre, CCDC, 12 Union Road, Cambridge CB21EZ, UK. Copies of the data can be obtained free of charge by quoting the depository number CCDC-2312629 for $[CHF_2CF_2OH_2][SbF_6]$ (**1**) (Fax: +44-1223-336-033; E-Mail: deposit@ccdc.cam.ac.uk, http://www.ccdc.cam.ac.uk). NMR samples were prepared by adding the HF solution to a small FEP tube under a nitrogen stream. The tube was sealed under vacuum and inserted into a standard NMR tube. For ^{1}H, ^{19}F, and ^{13}C measurements a JEOL ECX 400 and Bruker BioSpin GmbH AV400RT NMR spectrometer were used with acetone-d_6 as an external standard. For evaluation, MNOVA by Mestrelab was used.[8] Quantum chemical calculations were performed at the ωB97XD/aug-cc-pVTZ- and MP2/aug-cc-pVTZ-level of theory by Gaussian16.[9] GaussView 6.0 was used for visualization and illustration of the MEP calculations.[10] Hirshfeld surface analysis was performed with the CrystalExplorer software.[11,12]

Synthesis of $[CHF_2CF_2OH_2][SbF_6]$ (1): Antimony pentafluoride (1 mmol, 217 mg, 1.0 eq) and anhydrous hydrogen fluoride (100 mmol, 2 mL) were condensed into an FEP tube-reactor at −196 °C. To form the superacid, the mixture was warmed up to −50 °C and both components were mixed. After the mixture was cooled to −196 °C again, difluoroacetyl fluoride (1 mmol, 98.0 mg, 1.0 eq.) was condensed into the reaction vessel. Subsequently, the mixture was warmed up to −60 °C, and all components were reacted. Then, the temperature was reduced to −196 °C. The remaining HF was removed in dynamic vacuum at −78 °C. Compound (**1**) was obtained in quantitative yield as a colorless solid. Compound (**2**) was prepared analogously, using *a*DF instead of *a*HF.

Synthesis of $[CF_3CF_2OH_2][SbF_6]$ (3): Antimony pentafluoride (1 mmol, 217 mg, 1.0 eq) and anhydrous hydrogen fluoride (100 mmol, 2 mL) were condensed into an FEP tube-reactor at −196 °C. To form the superacid, the mixture was warmed up to −50 °C and both components were mixed. After the mixture was cooled to −196 °C again, trifluoroacetyl fluoride (1 mmol, 116 mg, 1.0 eq.) was condensed into the reaction vessel. Subsequently, the mixture was warmed up to −70 °C, and all components were reacted. For NMR measurements, the samples were prepared as mentioned before.

Table S1. Low-temperature Raman and IR spectra of $[CHF_2CF_2OH_2][SbF_6]$ (**1**) and $[CHF_2CF_2OD_2][SbF_6]$ (**2**) and calculated frequencies [cm^{-1}] of $[CHF_2CF_2OH_2]^+ \cdot 2HF$.

$[CHF_2CF_2OH_2][SbF_6]$ (**1**)		$[CHF_2CF_2OD_2][SbF_6]$ (**2**)		$[CHF_2CF_2OH_2]^+ \cdot 2HF$	Assignment		
Raman	IR	Raman	IR	calc.[a,b] (IR/Raman)[c]			
3055(25)		3055(50)	3053 m	2983(5/81)	ν_1	A	ν(C–H)
			2922 w	2957(1531/86)	ν_2	A	$\nu(OH_2)$
				2892(1873/42)	ν_3	A	$\nu(OH_2)$
		2821(4)					
2706(3)		2700(6)					
			2554 w				
			2498 w				
		2403(3)	2403 m				$\nu(OD_2)$
		2286(5)	2330 m				$\nu(OD_2)$
	1751 s						
			1709 w				
				1626(106/0)	ν_4	A	$\delta(OH_2)$
			1479 w				
			1460 w				
1362(13)	1364 s	1359(19)	1358 w	1406(14/1)	ν_5	A	ν(C–F) +δ(C–H) +$\gamma(OH_2)$
1328(4)	1329 s		1331 w	1325(15/2)	ν_6	A	δ(C–H)
		1285(6)	1286 m	1298(95/1)	ν_7	A	δ(C–H)
1251(11)	1256 s	1251(12)	1256 m	1235(236/2)	ν_8	A	ν(C–F) +δ(C–H)
		1205(3)	1196 m				
1164(5)	1151 s	1144(6)		1152(181/2)	ν_9	A	$\nu(C_H–F)$
1124(13)		1125(15)	1121 m	1102(6/4)	ν_{10}	A	$\nu(C_H–F)$
1112(12)	1113 s	1105(7)		1090(258/1)	ν_{11}	A	$\tau(OH_2)$
			1024 w				
			997 w				
	922 s						
		891(4)	889 m				
836(34)	835 s	816(30)	814 m	1045(89/3)	ν_{12}	A	ν(C–O)
				922(169/0)	ν_{13}	A	$\kappa(OH_2)$
		758(3)	756 w	755(67/5)	ν_{14}	A	ν(C–C) +ν(C–O)
				729(4/1)	ν_{15}	A	$\tau(OH_2)$
696(8)	699 vs			682(12/3)	ν_{16}	A	$\delta(CF_2)$
571(32)	569 s	565(19)	563 m	554(8/1)	ν_{17}	A	$\delta(CF_2)$
548(16)		552(20)		544(4/1)	ν_{18}	A	$\delta(COF_2)$
529(8)	527 s	522(20)	517 w	505(33/0)	ν_{19}	A	$\delta(COF_2)$
			449 w				

420(13)	417 s						
367(32)	364 s	367(37)	359 s	350(6/1)	ν_{20}	A	$\delta(CCF_2)$
257(7)		255(7)		308(40/0)	ν_{21}	A	δ(CCO)
206(7)		205(7)		205(5/0)	ν_{22}	A	$\tau(CF_2)$
				170(1/0)	ν_{23}	A	δ(CCO)
112(5)		112(6)		85(6/0)	ν_{24}	A	$\tau(CF_2)$
707(28)		702(16)					ν(Sb–F)
682(100)		683(100)					ν(Sb–F)
666(72)		666(75)	667 s				ν(Sb–F)
643(68)		642(64)	646 s				ν(Sb–F)
480(6)	488 s	484(8)	484 m				δ(Sb–F)
	426 s						δ(Sb–F)
	405 s	406(15)	409 m				δ(Sb–F)
	388 s		386 w				δ(Sb–F)
	378 s		372 s				δ(Sb–F)
337(7)		330(10)					δ(Sb–F)
322(7)		320(8)					δ(Sb–F)
282(44)		282(50)					δ(Sb–F)
268(31)		269(32)					δ(Sb–F)
193(5)		193(6)					δ(Sb–F)
175(3)		175(4)					δ(Sb–F)
152(5)		151(6)					δ(Sb–F)

[a] Calculated at ωB97XD/aug-cc-pVTZ-level of theory, [b] Frequencies are scaled with a factor of 0.956, [c] IR intensity in [km/mol] und Raman intensity in [Å⁴/u]. Abbreviations for IR intensities: vs = very strong, s = strong, m = medium, w = weak.

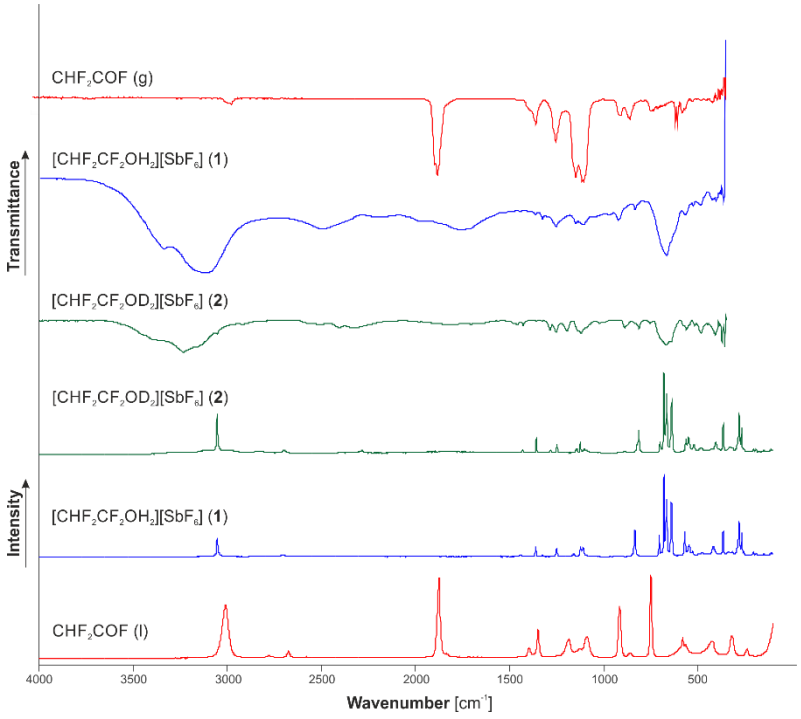

Figure S1. Low-temperature Raman and IR spectra of $[CHF_2CF_2OX_2][SbF_6]$ (**1**, **2**) (*X* = H, D) and vibrational spectra of CHF_2COF.

Table S2. Low-temperature Raman and IR spectra of CHF_2COF and calculated vibrational frequencies [cm^{-1}] of CHF_2COF.[13]

CHF_2COF Raman	CHF_2COF IR	CHF_2COF calc. [a,b] (IR/Raman)[c]	Assignment		
3010(65)	2980 m	2991(13/66)	ν_1	A'	ν_s(C–H)
2779(4)					ν(C–H)
2676(8)					
1876(98)	1886 vs	1864(245/15)	ν_2	A'	ν_s(C=O)
1840(6)					
1398(13)		1329(52/1)	ν_3	A'	δ_s(C–H)
1350(34)	1362 m	1323(11/2)	ν_{11}	A''	δ_{as}(C–H)
1250(4)	1256 s	1230(201/2)	ν_4	A'	ν_s(C–F)
1188(23)					
	1151 vs				
1128(11)	1117 vs	1097(63/4)	ν_5	A'	ν_s(CF_2)
1090(27)	1107 vs	1082(217/3)	ν_{12}	A''	ν_{as}(CF_2)
919(64)	916 m				
862(7)	864 m	834(81/7)	ν_6	A'	ν_s(C–C)
751(100)	748 m	739(20/0)	ν_{13}	A''	κ_{as}(COF)
699(3)	704 m	685(50/2)	ν_7	A'	δ_s(COF)
	619 m				
	611 m				
581(27)	581 m	563(15/2)	ν_8	A'	δ_s(CF_2)
569(18)	571 m			A''	δ(CF_2)
501(7)					
421(21)	426 m	397(2/2)	ν_9	A'	δ_s(CCO)
322(28)					
240(12)		241(6/0)	ν_{10}	A'	δ_s(CCF)
211(4)		228(6/0)	ν_{14}	A''	γ_{as}(CF_2)
		44(4/1)	ν_{15}	A''	*lattice*

[a] Calculated at ωB97XD/aug-cc-pVTZ-level of theory, [b] Frequencies are scaled with a factor of 0.956, [c] IR intensity in [km/mol] und Raman intensity in [$Å^4$/u]. Abbreviations for IR intensities: vs = very strong, s = strong, m = medium, w = weak.

Table S3. Low-temperature Raman and IR spectra of CF_3COF and calculated vibrational frequencies [cm^{-1}] of CF_3COF.[14]

CF_3COF Raman	CF_3COF IR	CF_3COF calc. [a,b] (IR/Raman)[c]	Assignment		
1888(27)	1896 w	1889(244/15)	ν_1	A'	ν_s(C=O)
1342(7)	1331 w	1285(86/2)	ν_2	A'	ν_s(C–F)
1244(3)	1252 s	1210(333/1)	ν_3	A'	ν_s(C–F)
	1211 m				
1193(4)	1200 s	1158(288/2)	ν_{11}	A''	ν_{as}(C–F)
1092(3)	1097 vs	1072(276/1)	ν_4	A'	ν_s(C–F)
809(100)	803 w	783(6/10)	ν_5	A'	ν_s(C–C)
768(4)					
759(4)	760 w	746(19/0)	ν_{12}	A''	κ_{as}(COF)
	700 w				
692(5)	692 w	672(47/0)	ν_6	A'	δ_s(COF)
595(9)		571(1/1)	ν_7	A'	δ_s(CF_2)
519(6)		500(7/1)	ν_{13}	A''	δ_{as}(CF_2)
427(22)		408(2/1)	ν_8	A'	δ_s(CCF)
387(40)		368(0/2)	ν_9	A'	δ_s(CCF)
245(11)		232(5/0)	ν_{14}	A''	τ_{as}(CF_2)
		219(3/0)	ν_{10}	A'	δ_s(CCF)
		43(1/0)	ν_{15}	A''	τ_{as}(COF)

[a] Calculated at ωB97XD/aug-cc-pVTZ-level of theory, [b] Frequencies are scaled with a factor of 0.956, [c] IR intensity in [km/mol] und Raman intensity in [$Å^4$/u]. Abbreviations for IR intensities: vs = very strong, s = strong, m = medium, w = weak.

Table S4. X-ray data and refinement of $[CHF_2CF_2OH_2][SbF_6]$ (**1**).

	$[CHF_2CF_2OH_2][SbF_6]$ (**1**)
formula	$C_2H_3F_{10}OSb$
M_r [g mol^{-1}]	354.79
crystal size [mm^3]	0.373 x 0.154 x 0.118
crystal system	triclinic
space group	$P\overline{1}$
a [Å]	6.3267(5)
b [Å]	7.8117(5)
c [Å]	8.5217(5)
α [°]	85.971(5)
β [°]	87.605(6)
γ [°]	85.482(6)
V [Å^3]	418.54(5)
Z	2
ρ_{calc} [g cm^{-3}]	2.815
μ [mm^{-1}]	3.473
$\lambda_{MoK\alpha}$ [Å]	0.71073
F(000)	328
T [K]	101(2)
hkl range	−9:9, −11:11, −12:12
refl. measured	8217
refl. unique	2548
R_{int}	0.0504
parameters	139
R(F)/wR(F²) [a] (all reflexions)	0.0349/0.0597
weighting scheme [b]	0.0173/0.0000
S (GoF) [c]	1.081
residual density [e Å^{-3}]	1.199/−1.246
device type	Oxford XCalibur
solution	SHELXT[15]
refinement	SHELXL-2018/3[16]
CCDC	2312629

[a] $R_1 = \Sigma\,||F_0|-|F_C||/\Sigma|F_0|$;
[b] $wR_2 = [\Sigma[w(F^2_0 - F^2_C)^2]/\Sigma(F_0)^2]]^{1/2}$; $w = [\sigma^2_C(F^2_0) + (xP)^2 + yP]^{-1}$; $P = (F^2_0 + 2F^2_C)/3$;
[c] GooF = $[\Sigma[(F^2_0 - F^2_C)^2]/(n\text{-}p)]^{1/2}$ (n = number of relexions; p = total numbers of parameters).

Table S5. Bond lengths [Å] and bond angles [°] of $[CHF_2CF_2OH_2][SbF_6]$ (**1**) as well as donor-acceptor distances of **1**. Symmetry codes: *i* = –1+*x*, *y*, *z*; *ii* = 1–*x*, 1–*y*, 1–*z*; *iii* = *x*, 1+*y*, *z*; *iv* = 1–*x*, –*y*, 2–z; *v* = 1–*x*, 1–*y*, 2–*z*.

$[CHF_2CF_2OH_2][SbF_6]$ (**1**)			
Bond lengths [Å]			
C1–C2	1.524(5)	Sb1–F5	1.925(2)
C1–F1	1.318(4)	Sb1–F6	1.914(2)
C1–F2	1.325(4)	Sb1–F7	1.854(2)
C2–F3	1.341(4)	Sb1–F8	1.853(2)
C2–F4	1.346(4)	Sb1–F9	1.857(2)
C1–O1	1.424(4)	Sb1–F10	1.862(2)
Bond angles [°]			
C2–C1–O1	109.1(3)	F5–Sb1–F9	88.45(8)
F1–C1–F2	110.0(3)	F5–Sb1–F10	87.20(8)
F1–C1–C2	111.9(3)	F6–Sb1–F7	88.35(9)
F2–C1–C2	110.6(3)	F6–Sb1–F8	90.97(9)
F3–C2–F4	108.5(3)	F6–Sb1–F9	87.29(9)
F3–C2–C1	108.1(3)	F6–Sb1–F10	174.37(8)
F4–C2–C1	107.2(3)	F7–Sb1–F8	92.69(9)
F1–C1–O1	106.3(3)	F7–Sb1–F9	173.57(9)
F2–C1–O1	108.8(2)	F7–Sb1–F10	92.02(9)
F5–Sb1–F6	87.21(8)	F8–Sb1–F9	92.10(9)
F5–Sb1–F7	86.62(8)	F8–Sb1–F10	94.62(9)
F5–Sb1–F8	178.08(8)	F9–Sb1–F10	91.86(9)
Dihedral angles [°]			
F3–C2–C1–F1	55.0(3)	F4–C2–C1–F2	–65.2(3)
F4–C2–C1–F1	171.8(2)	F3–C2–C1–O1	–62.4(3)
F3–C2–C1–F2	178.0(2)	F4–C2–C1–O1	54.5(3)
Donor-acceptor distances [Å]			
O1(–H1)···F6*i*	2.471(3)	O1···F9*iv*	2.689(3)
O1(–H2)···F5	2.452(3)	F5···F3*v*	2.888(3)
C2(–H3)···F7*ii*	3.129(4)	F5···F9iv	2.890(2)
C2(–H3)···F10*iii*	3.166(4)		

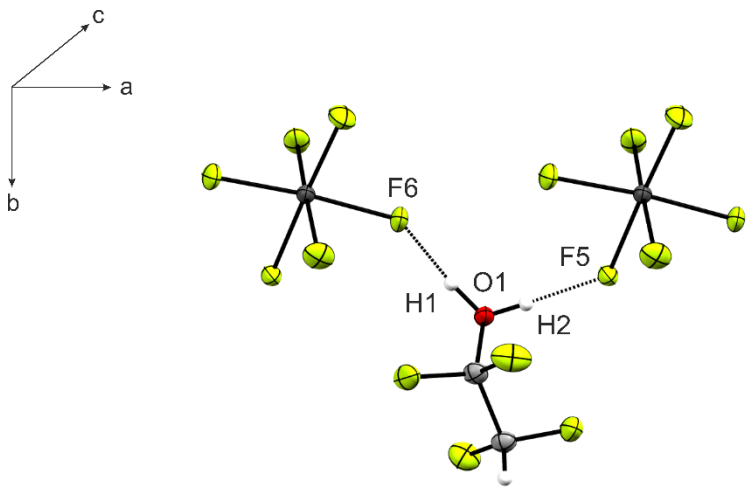

Figure S2. Chains along the *a*-axis of **1** (displacement ellipsoids with 50% probability).

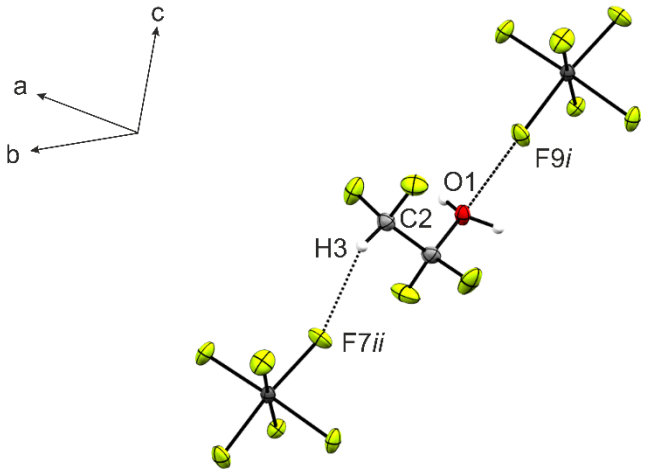

Figure S3. Chains along the *c*-axis of **1** (displacement ellipsoids with 50% probability).
Symmetry codes: *i* = 1–*x*, –*y*, 2–*z*; *ii* = 1–*x*, 1–*y*, 1–*z*.

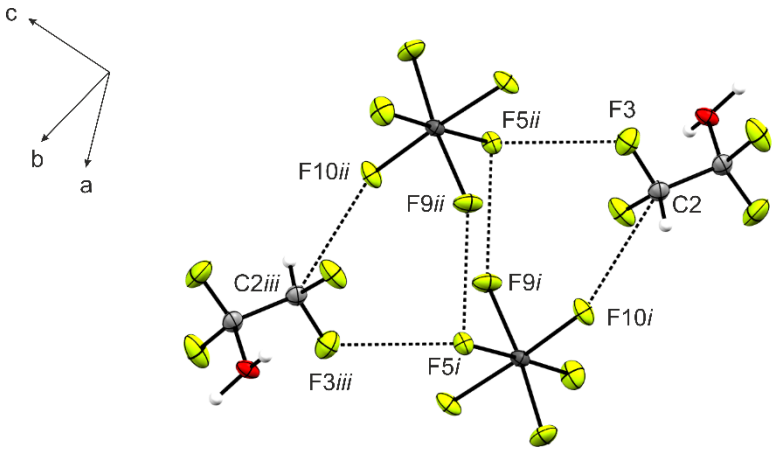

Figure S4. Intermolecular F···F contacts of **1** (displacement ellipsoids with 50% probability).
Symmetry codes: *i* = *x*, 1+*y*, *z*; *ii* = 1–*x*, 1–*y*, 2–*z*; *iii* = 1+*x*, 2–*y*, 2–*z*.

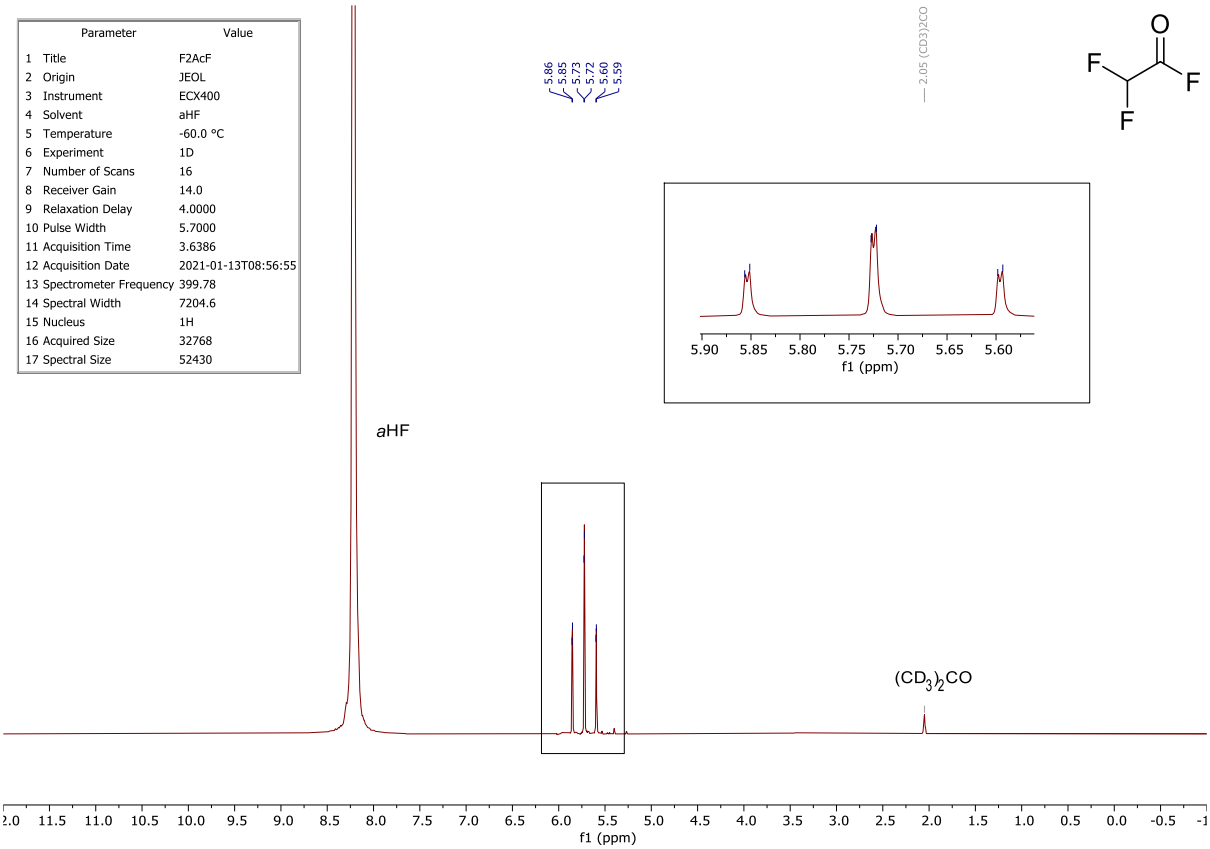

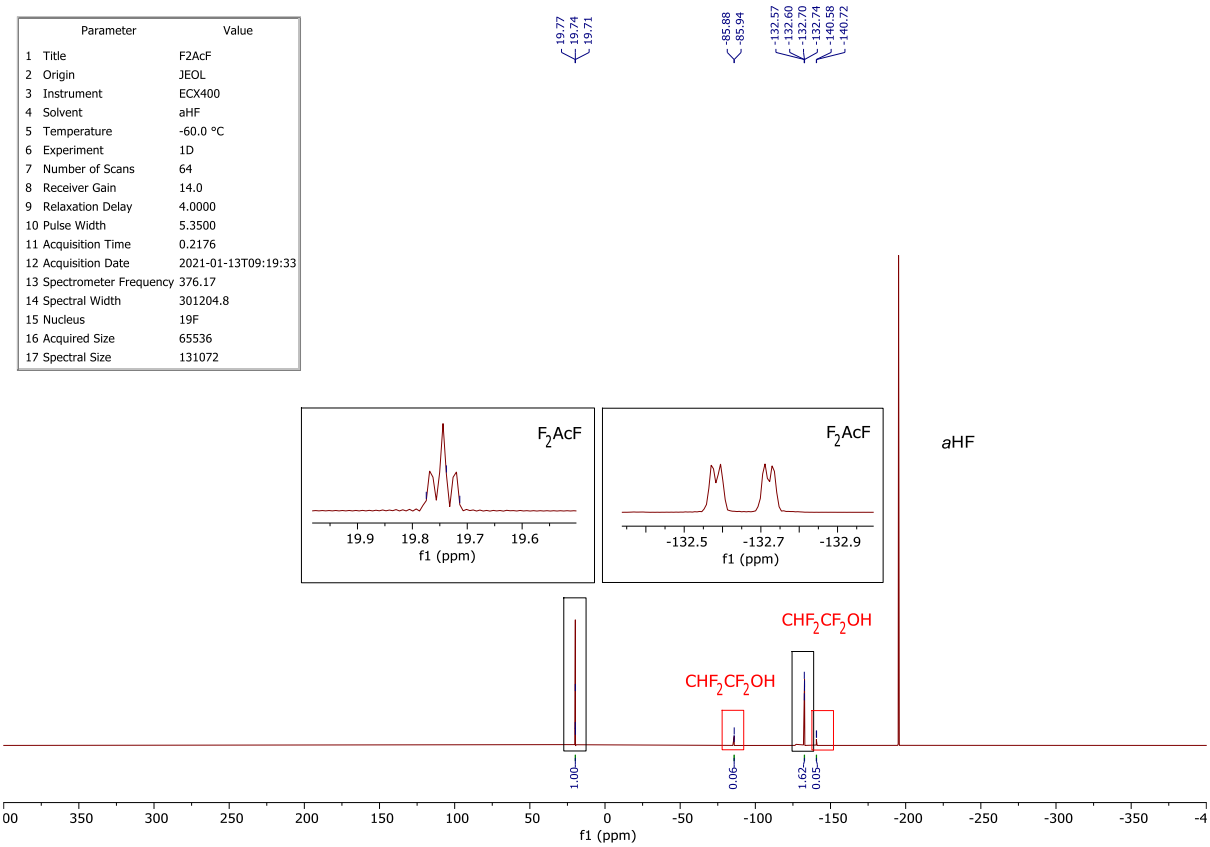

Figure S5. ^{1}H and ^{19}F NMR spectra of CHF_2COF in *a*HF at −60 °C.

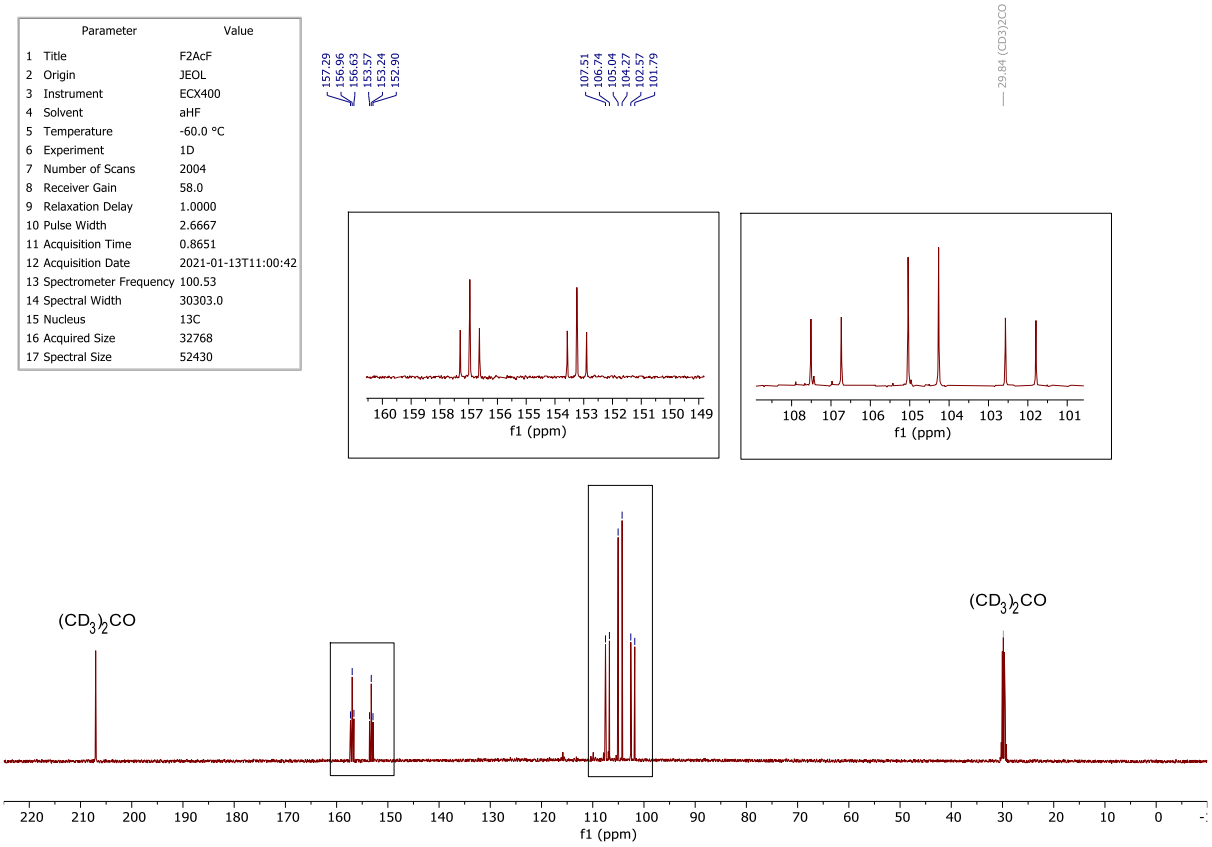

Figure S6. ^{13}C NMR spectrum of CHF_2COF in *a*HF at –60 °C.

CHF_2COF:

^{1}H NMR [400 MHz, $(CD_3)_2CO$)]: δ = 5.72 (td, *J* = 51.5, 2.1 Hz, CHF_2).

^{19}F NMR [376 MHz, $(CD_3)_2CO$)]: δ = 19.74 (t, *J* = 11.5 Hz, COF), –132.65 (dd, *J* = 50.6, 11.5 Hz, CHF_2).

^{13}C NMR [101 MHz, $(CD_3)_2CO$)]: δ = 155.1 (dt, *J* = 374.5, 33.8 Hz, COF), 104.7 (td, *J* = 248.2, 77.7 Hz, CHF_2).

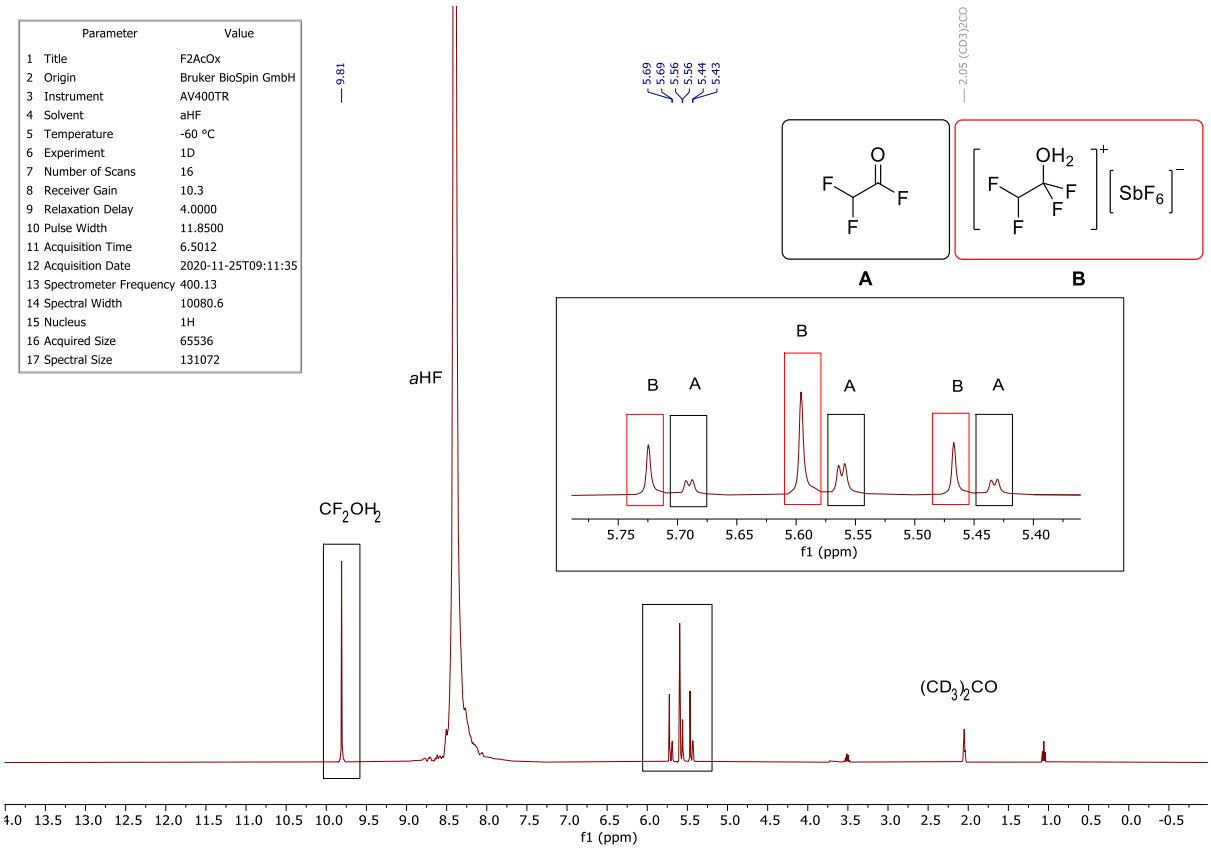

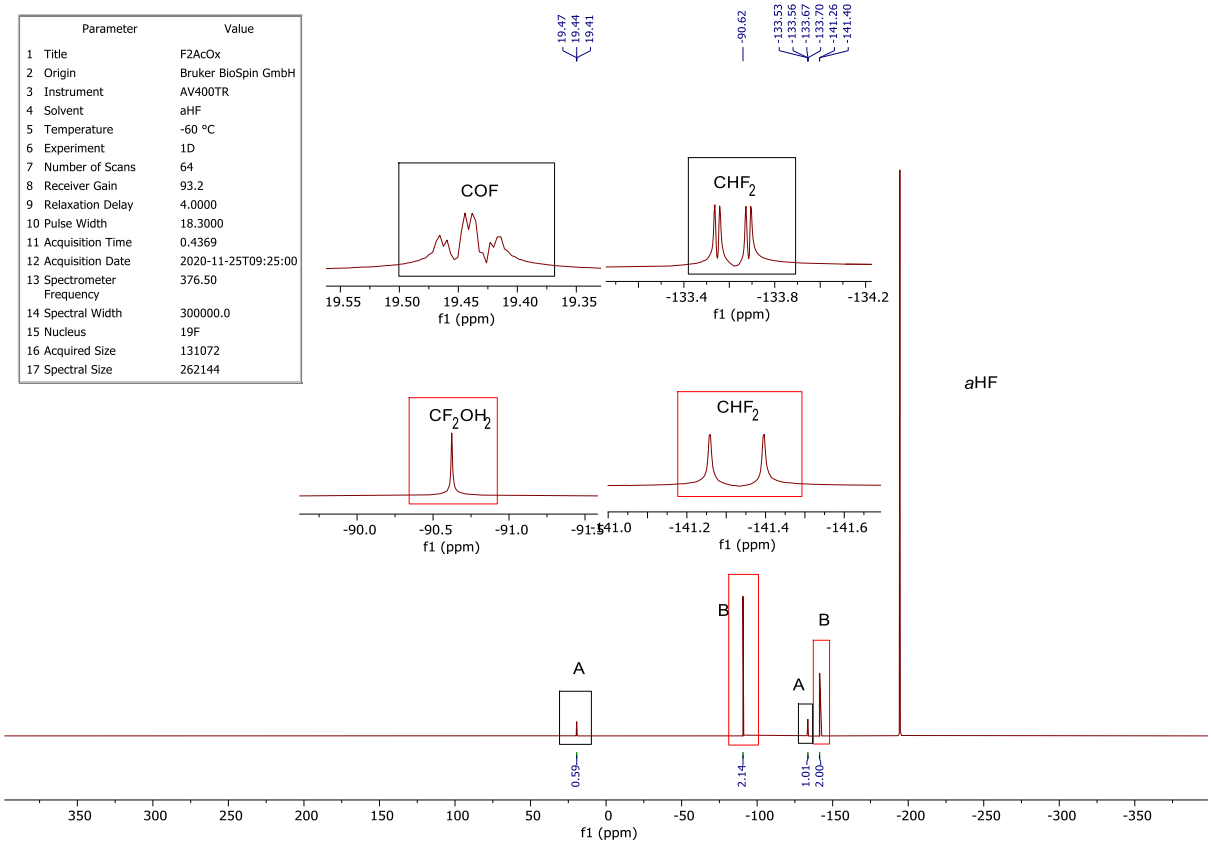

Figure S7. ^{1}H and ^{19}F NMR spectra of CHF_2COF in HF/SbF_5 at –60 °C.

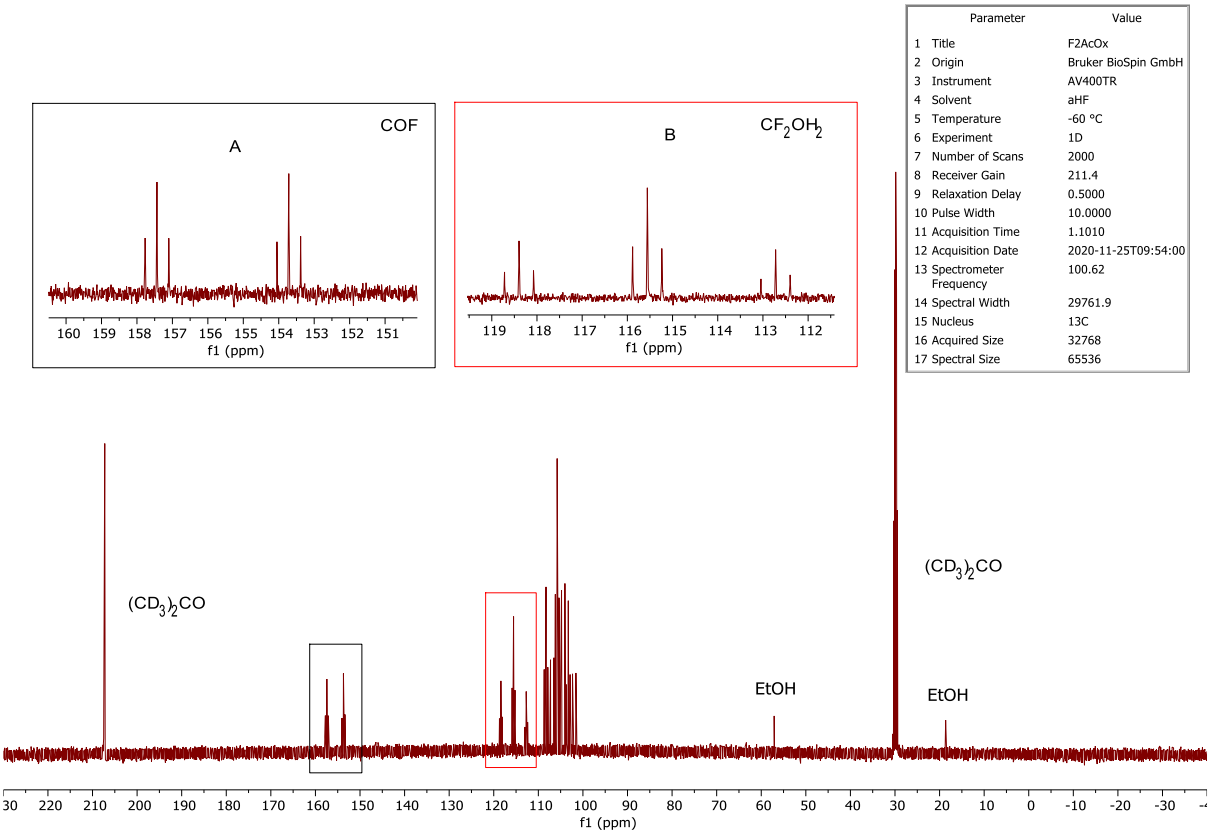

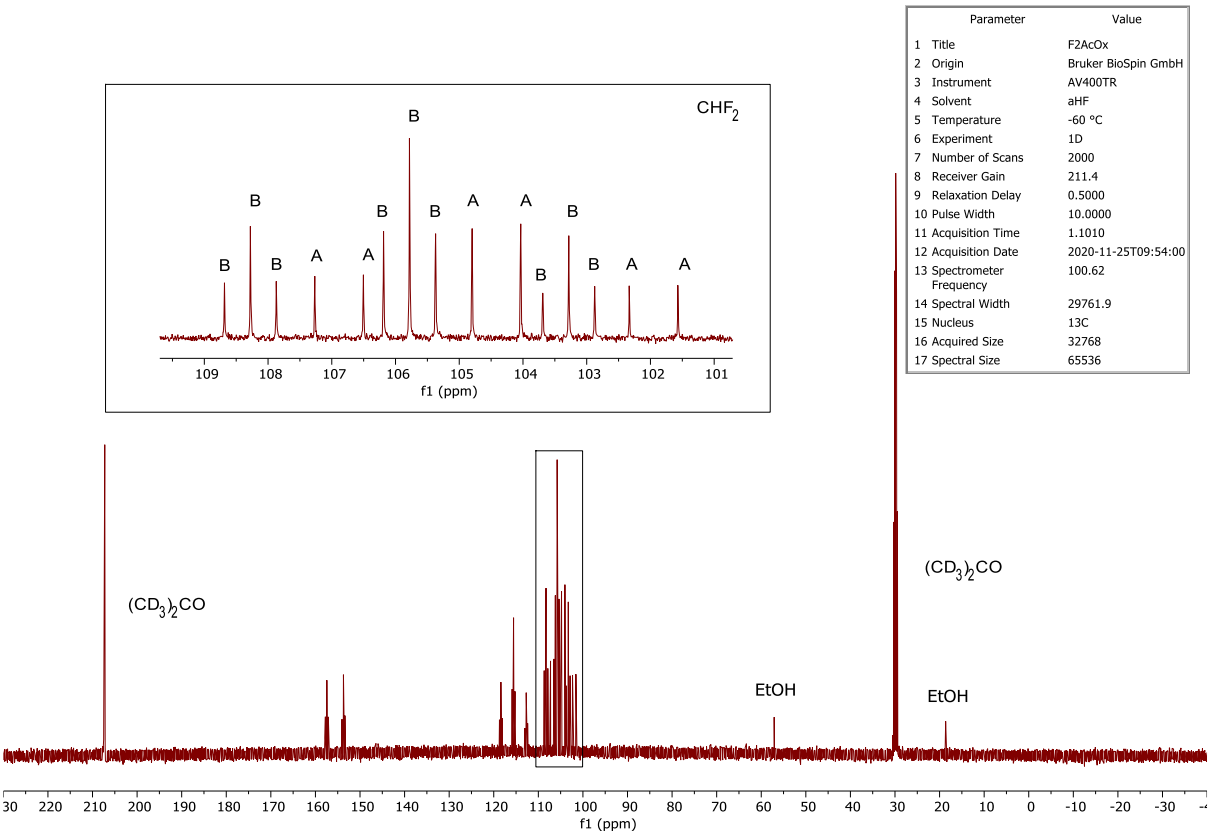

Figure S8. ^{13}C NMR spectra of CHF_2COF in HF/SbF_5 at –60 °C.

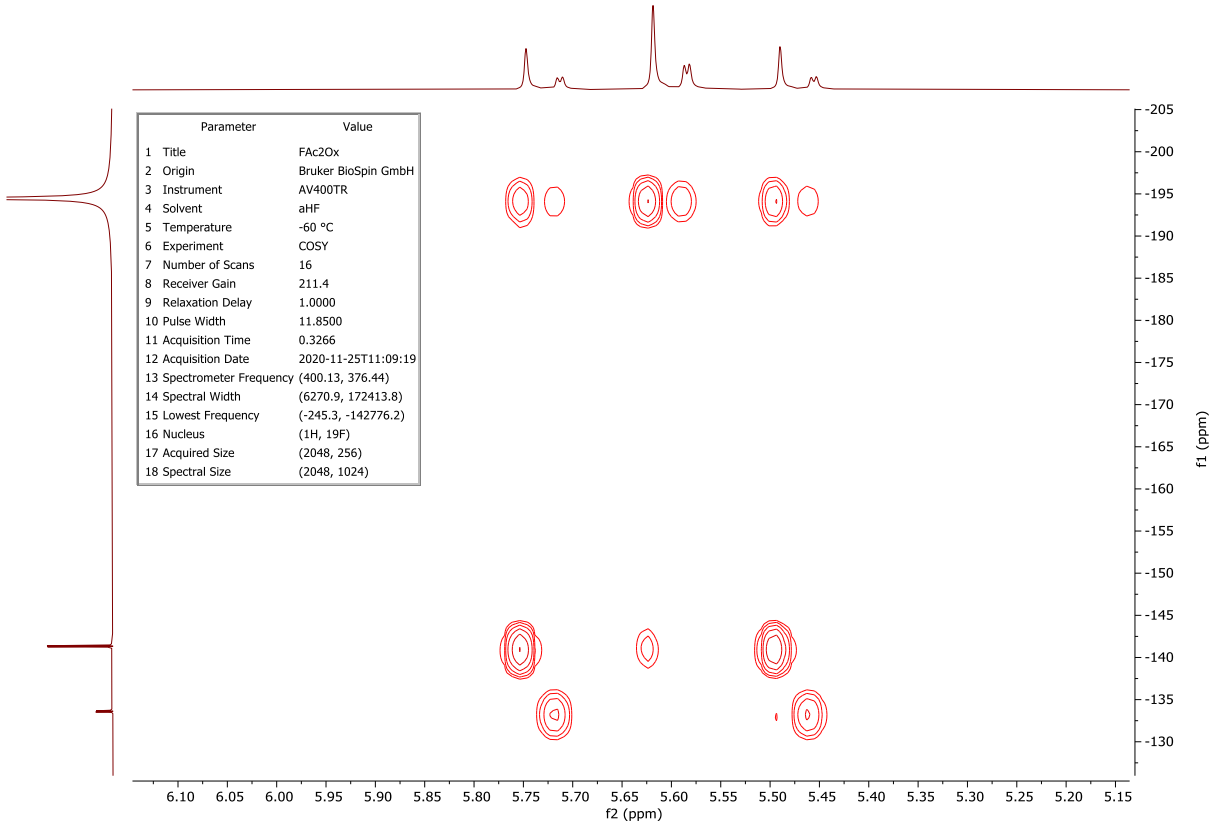

Figure S9. ^{1}H-^{19}F-COSY NMR spectrum of CHF_2COF in HF/SbF_5 at –60 °C.

CHF_2COF (black):

^{1}H NMR [400 MHz, $(CD_3)_2CO$)]: δ = 5.56 (td, *J* = 51.5, 2.2 Hz, CHF_2).

^{19}F NMR [376 MHz, $(CD_3)_2CO$)]: δ = 19.43 (t, *J* = 11.4 Hz, COF), –133.62 (dd, *J* = 51.5, 12.6 Hz, CHF_2).

^{13}C NMR [101 MHz, $(CD_3)_2CO$)]: δ = 155.6 (dt, *J* = 374.2, 33.6 Hz, COF), 104.4 (td, *J* = 248.4, 76.7 Hz, CHF_2).

$[CHF_2CF_2OH_2][SbF_6]$ (red):

^{1}H NMR [400 MHz, $(CD_3)_2CO$)]: δ = 9.81 (s, CF_2OH_2), 5.60 (t, *J* = 51.5 Hz, CHF_2).

^{19}F NMR [376 MHz, $(CD_3)_2CO$)]: δ = –90.62 (s, CF_2OH_2), –129.19 (s, $[SbF_6]^-$), –141.33 (d, *J* = 51.5 Hz, CHF_2).

^{13}C NMR [101 MHz, $(CD_3)_2CO$)]: δ = 115.6 (tt, *J* = 285.6, 32.2 Hz, CF_2OH_2), 105.8 (tt, *J* = 251.1, 40.9 Hz, CHF_2).

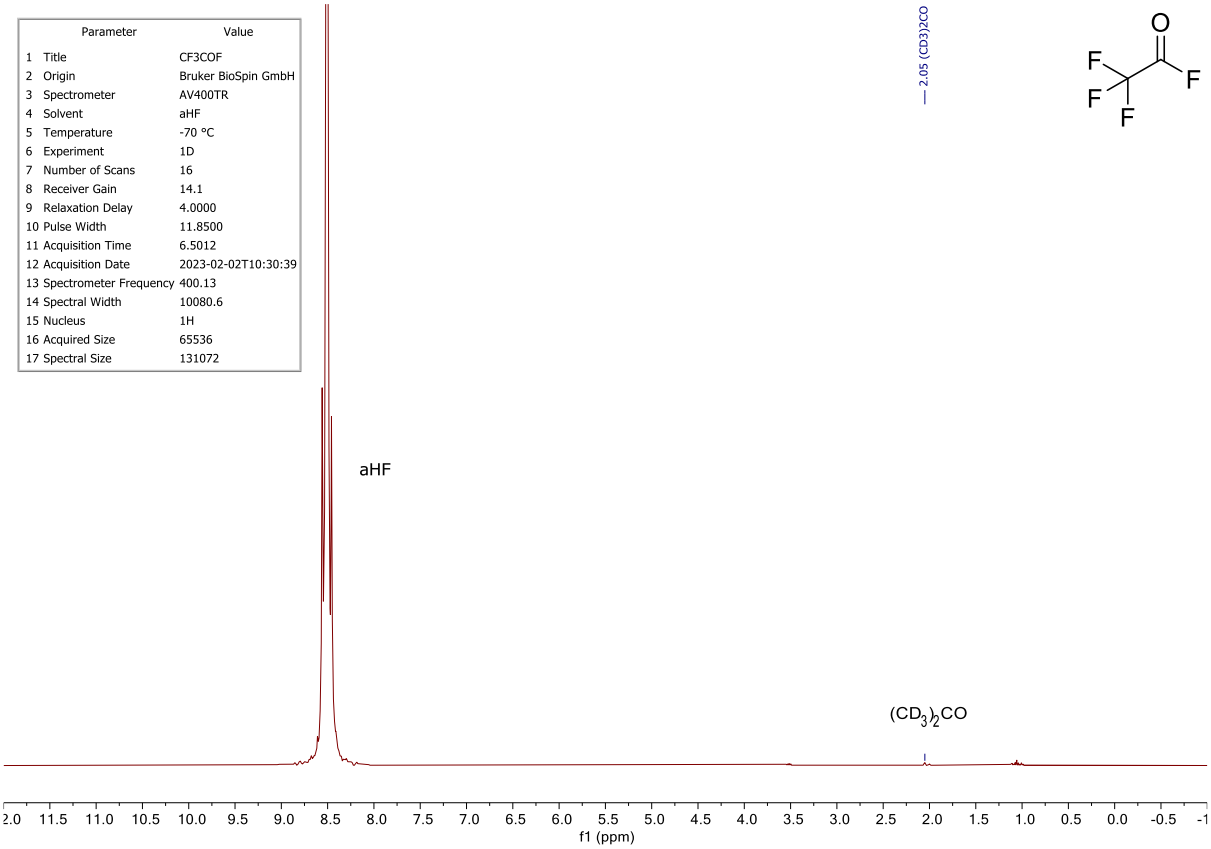

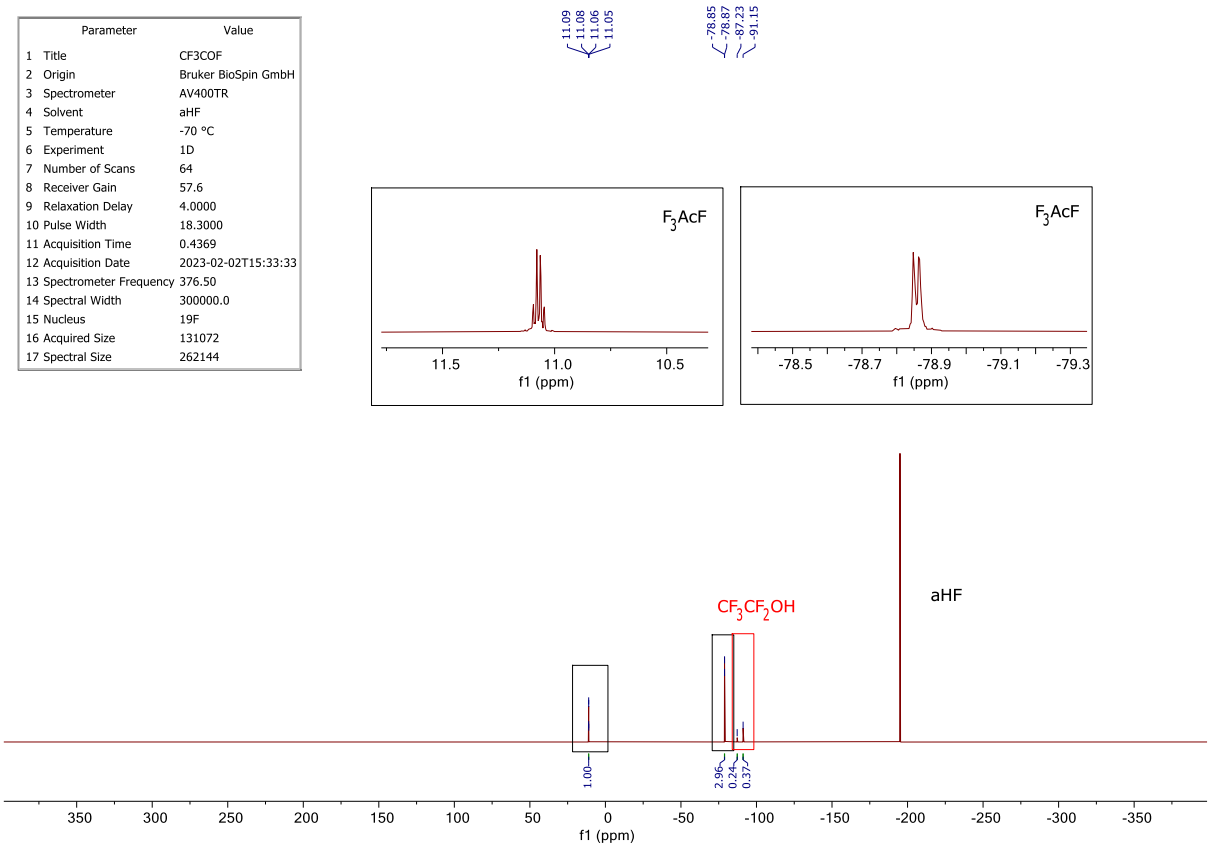

Figure S10. ^{1}H and ^{19}F NMR spectra of CF_3COF in *a*HF at −70 °C.

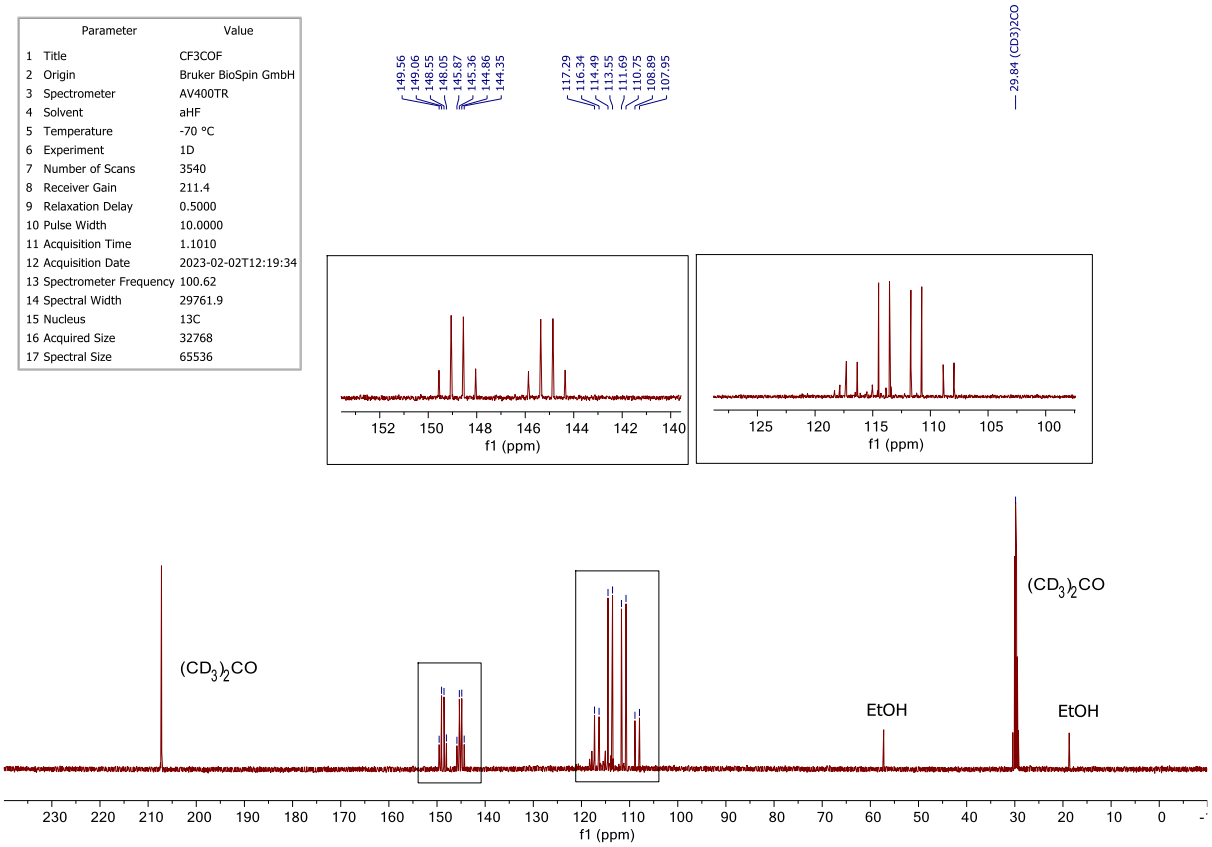

Figure S11. ^{13}C NMR spectrum of CF_3COF in *a*HF at −70 °C.

CF_3COF:

^{19}F NMR [376 MHz, $(CD_3)_2CO$)]: δ = 11.07 (q, *J* = 5.8 Hz, COF), –78.86 (d, *J* = 5.8 Hz, CF_3).

^{13}C NMR [101 MHz, $(CD_3)_2CO$)]: δ = 147.0 (dq, *J* = 371.5, 50.6 Hz, COF), 112.6 (qd, *J* = 281.6, 94.9 Hz, CF_3).

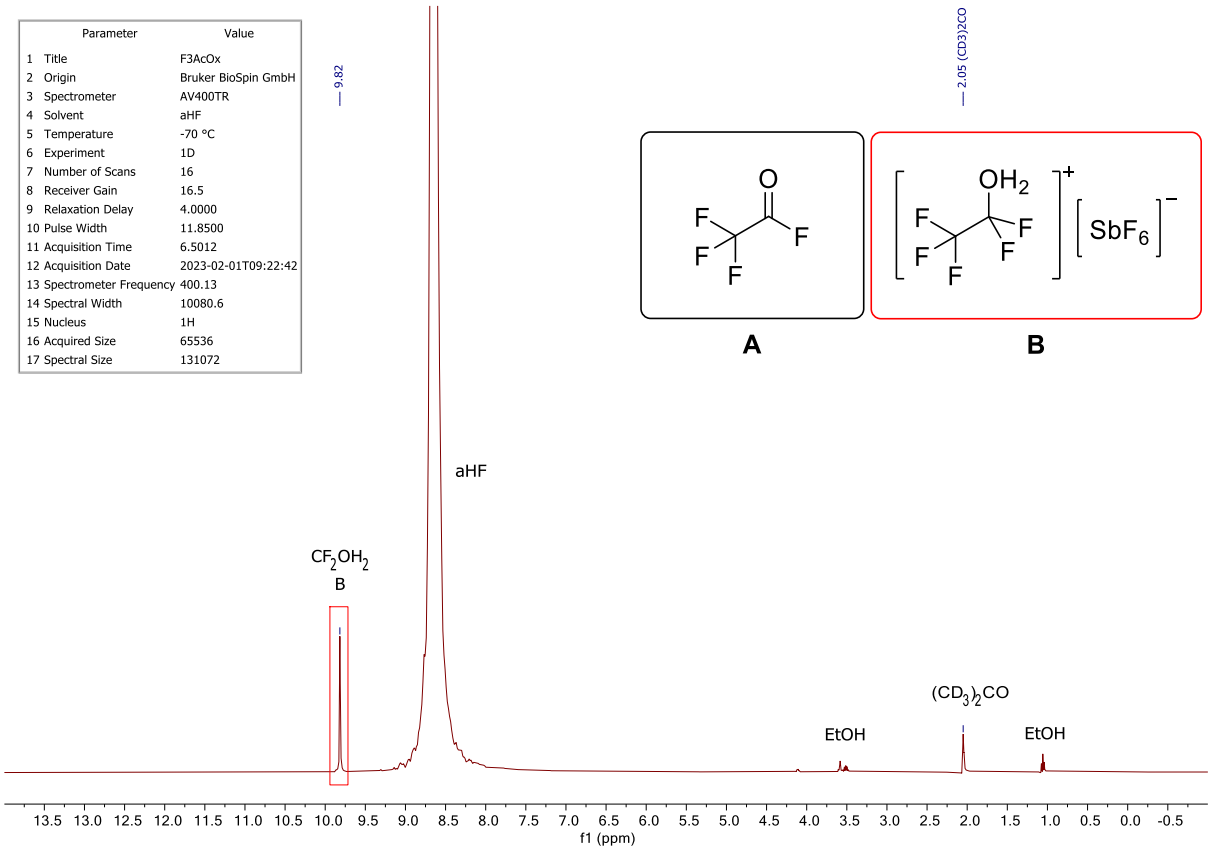

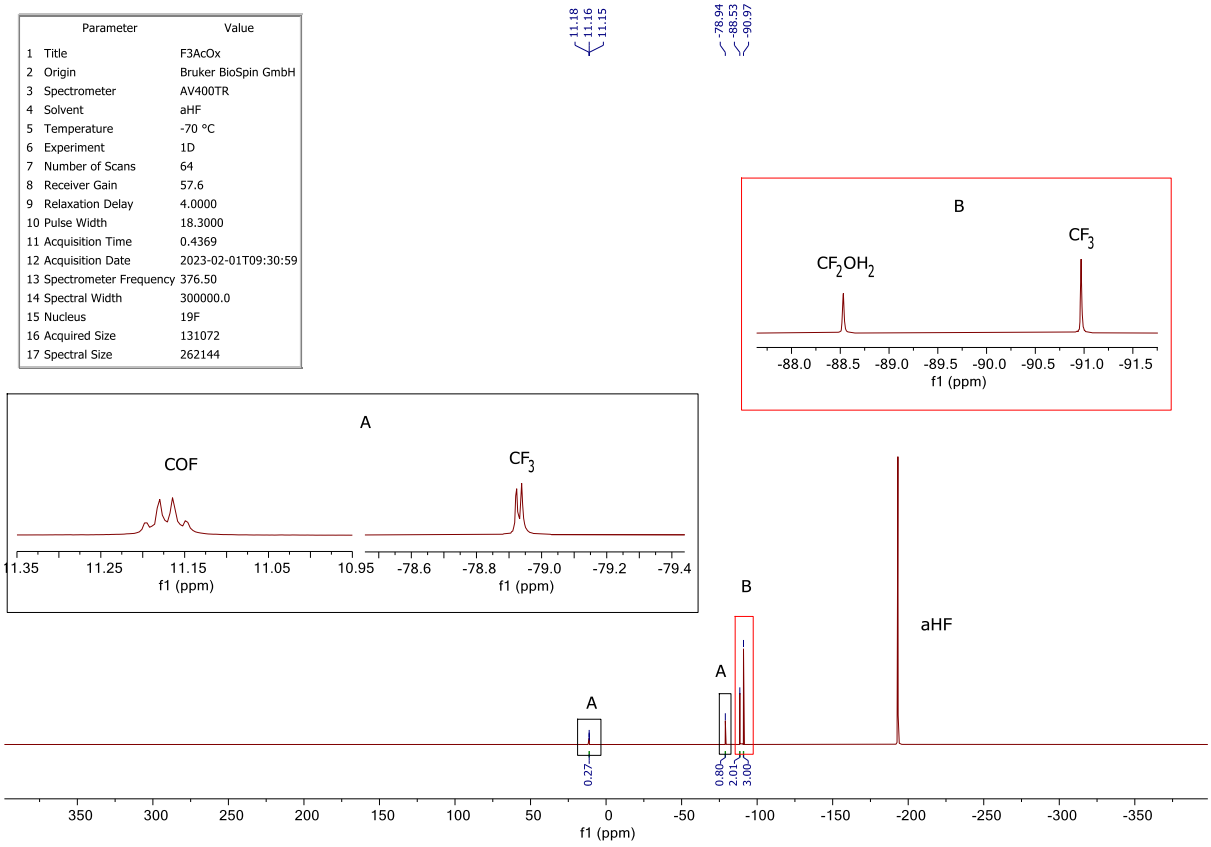

Figure S12. ^{1}H and ^{19}F NMR spectra of CF_3COF in HF/SbF_5 at −70 °C.[17]

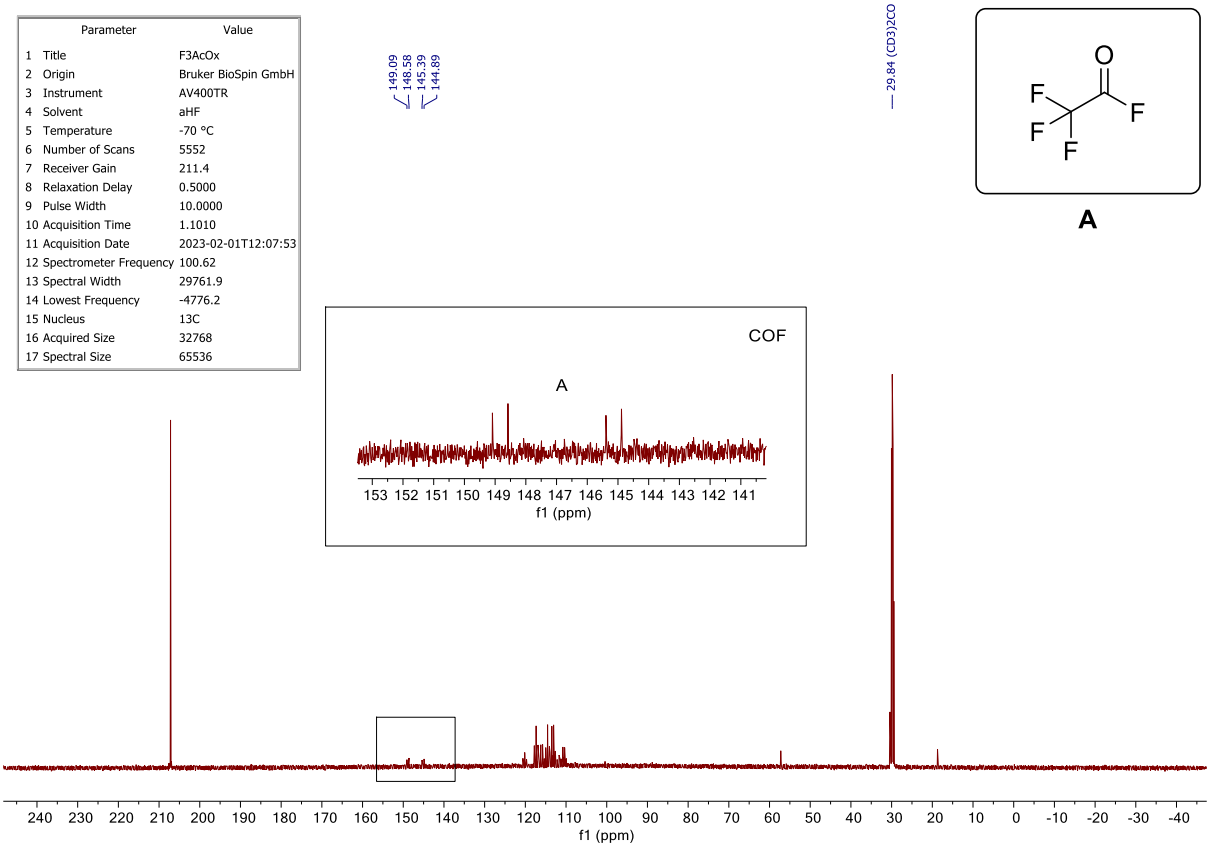

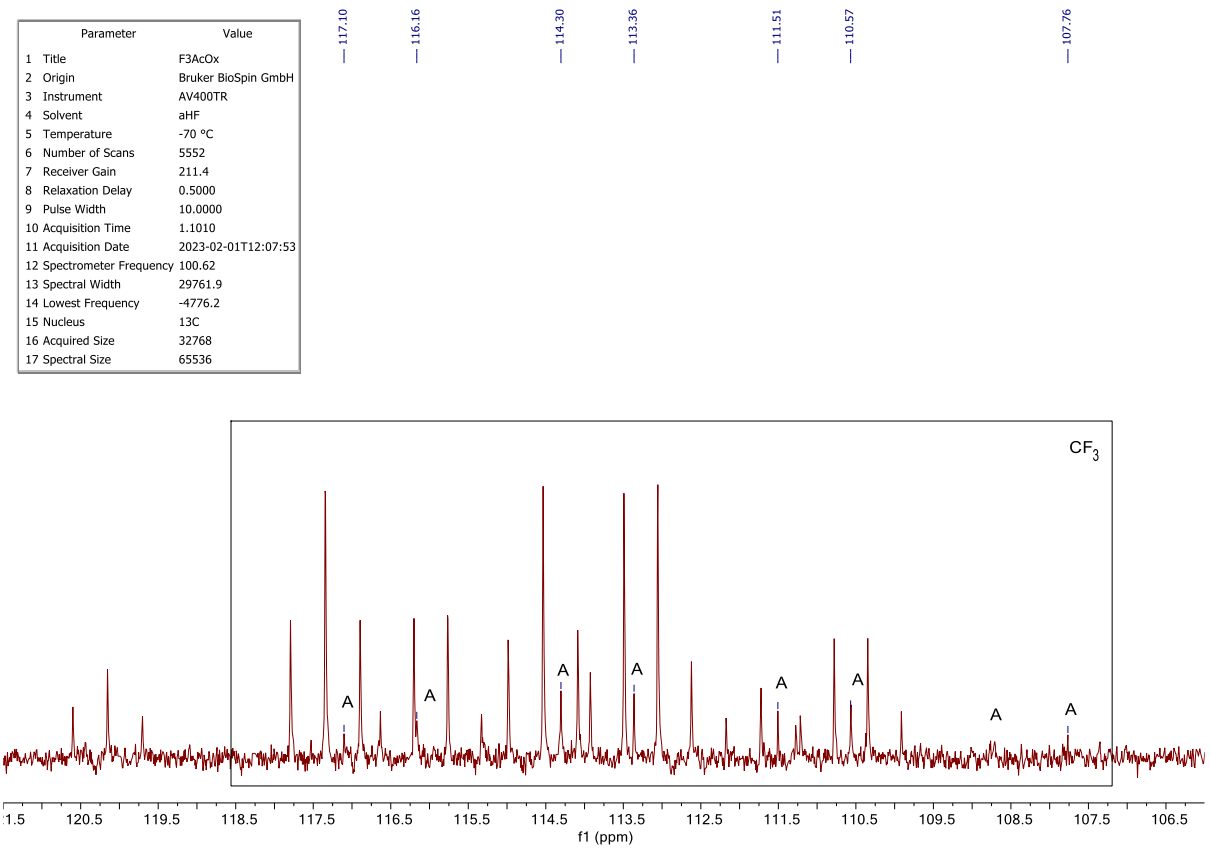

Figure S13. ^{13}C NMR spectra of CF_3COF in HF/SbF_5 at –70 °C.[17]

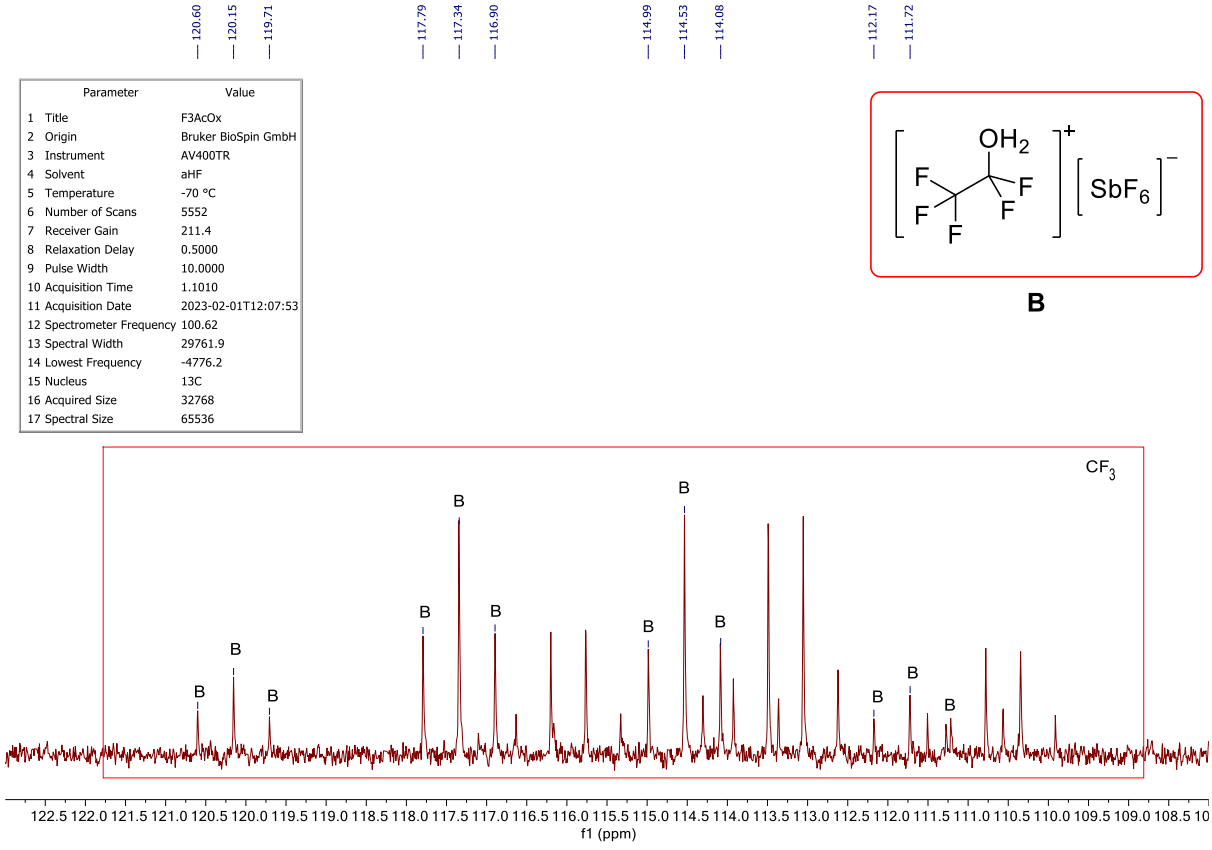

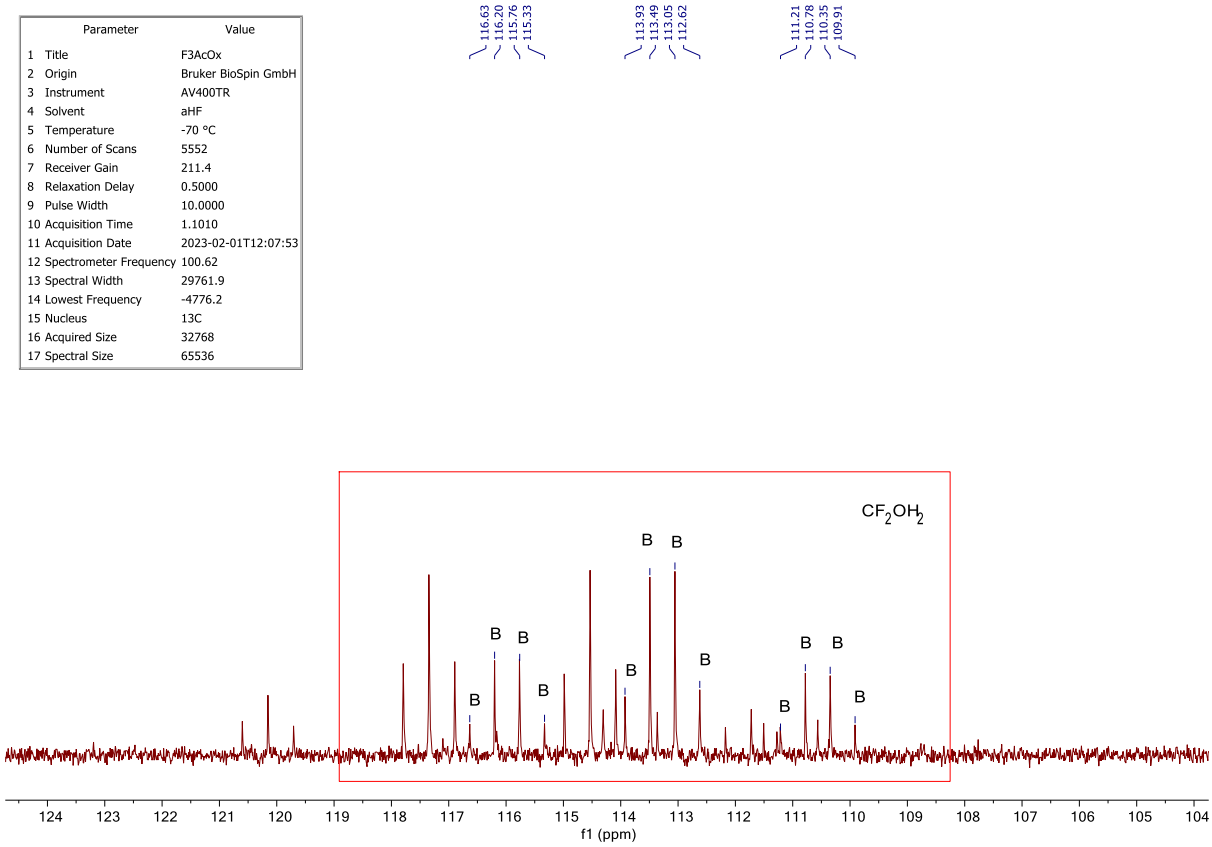

Figure S14. ^{13}C NMR spectra of CF_3COF in HF/SbF_5 at –70 °C.[17]

CF_3COF (black):

^{19}F NMR [376 MHz, $(CD_3)_2CO$)]: δ = 11.17 (q, *J* = 5.7 Hz, COF), –78.93 (d, *J* = 5.7 Hz, CF_3).

^{13}C NMR [101 MHz, $(CD_3)_2CO$)]: δ = 147.0 (dd, *J* = 372.2, 50.6 Hz, COF), 112.4 (qd, *J* = 281.3, 94.5 Hz, CF_3).

$[CF_3CF_2OH_2][SbF_6]$ (red):

^{1}H NMR [400 MHz, $(CD_3)_2CO$)]: δ = 9.82 (s, CF_2OH_2).

^{19}F NMR [376 MHz, $(CD_3)_2CO$)]: δ = –88.53 (s, CF_2OH_2), –90.97 (s, CF_3), –128.48 (s, $[SbF_6]^-$).

^{13}C NMR [101 MHz, $(CD_3)_2CO$)]: δ = 115.9 (qt, *J* = 282.9, 45.0 Hz, CF_3), 113.3 (tq, *J* = 272.6, 43.7 Hz, CF_2OH_2).

Quantum Chemical Calculations

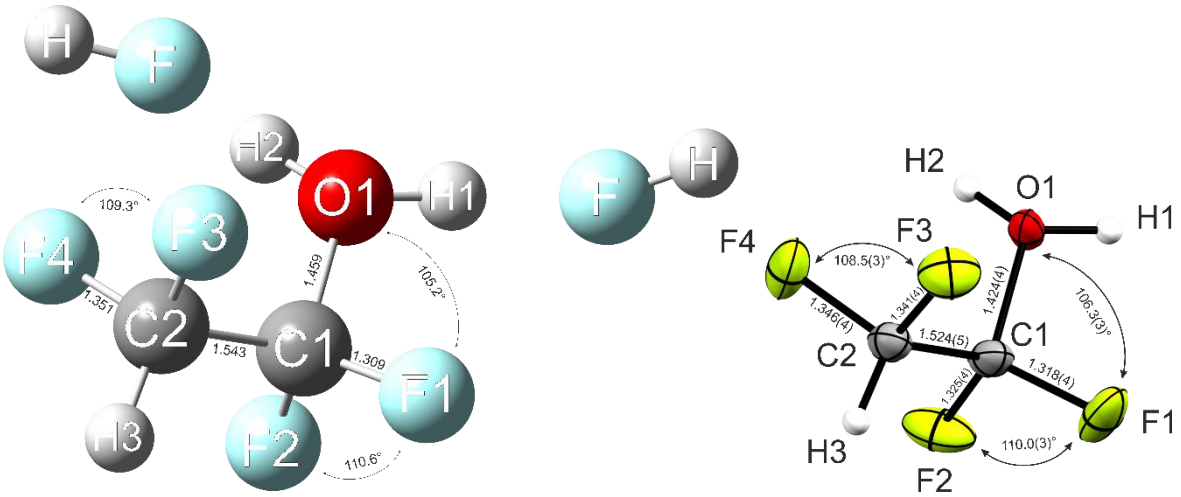

Figure S15. Calculated gas phase structure of $[CHF_2CF_2OH_2]^+ \cdot 2HF$. Bond lengths are given in [Å]. Calculated at the ωB97XD/aug-cc-pVTZ-level of theory.

Table S6. Standard orientations of CHF_2COF.

CHF_2COF							
ωB97XD/aug-cc-pVTZ				MP2/aug-cc-pVTZ			
Atom	Coordinates [Å]			Atom	Coordinates [Å]		
	X	Y	Z		X	Y	Z
F	0.934053	1.027379	0.652619	F	−1.001457	1.206921	0.009687
O	1.743417	−0.702603	−0.441611	O	−1.701270	−0.881980	−0.007078
C	0.813814	−0.080707	−0.088554	C	−0.814944	−0.108204	−0.000988
C	−0.662753	−0.341502	−0.351587	C	0.675906	−0.463051	−0.003975
F	−1.199666	−0.829486	0.786875	F	1.258593	0.074352	−1.092910
F	−1.295971	0.819634	−0.622324	F	1.258302	0.055203	1.094320
H	−0.800049	−1.003665	−1.180797	H	0.805446	−1.544928	−0.013464

Table S7. Standard orientations of CF_3COF.

CF_3COF							
ωB97XD/aug-cc-pVTZ				MP2/aug-cc-pVTZ			
Atom	Coordinates [Å]			Atom	Coordinates [Å]		
	X	Y	Z		X	Y	Z
F	1.541514	1.022314	−0.014292	F	1.505837	−1.048963	−0.000008
O	1.517571	−1.180516	0.007925	O	1.557370	1.156790	−0.000008
C	0.934020	−0.158898	−0.002362	C	0.949285	0.155117	−0.000010
C	−0.590757	−0.005234	−0.004040	C	−0.592042	0.016548	−0.000006
F	−1.090790	−0.521112	1.135232	F	−0.986025	−0.651555	−1.081120
F	−0.905509	1.303253	−0.057120	F	−0.986007	−0.651201	1.081342
F	−1.123008	−0.645687	−1.066597	F	−1.156297	1.209018	−0.000196

Table S8. Standard orientations of $[CHF_2CF_2OH_2]^+\cdot 2HF$ and $[CF_3CF_2OH_2]^+\cdot 2HF$.

$[CHF_2CF_2OH_2]^+\cdot 2HF$				**$[CF_3CF_2OH_2]^+\cdot 2HF$**			
ωB97XD/aug-cc-pVTZ				ωB97XD/aug-cc-pVTZ			
Atom	Coordinates [Å]			Atom	Coordinates [Å]		
	X	Y	Z		X	Y	Z
F	−0.351135	2.663226	−0.177546	F	2.372447	−2.017225	−0.335153
F	1.706275	−1.077677	−1.153021	F	−0.551544	−1.080263	1.458106
F	−0.377965	−1.731401	0.420533	O	1.091485	0.000464	0.480497
F	−0.041857	−1.731401	1.649537	C	−1.189510	−0.000366	−0.538069
O	−0.627897	0.247900	−0.496373	C	−0.344182	−0.000424	0.743629
F	1.955394	−0.799121	−0.070855	H	1.476126	0.843662	0.093708
C	1.592428	−0.491663	0.047262	F	−0.552826	1.078176	1.459386
C	0.121803	−0.511870	0.446741	H	1.476801	−0.842324	0.093813
H	2.121712	−0.867185	0.671287	F	2.368480	2.020976	−0.332500
H	−1.460390	−0.051904	−0.552685	H	2.104339	2.806924	−0.474333
H	−0.503529	1.073225	−0.489790	H	2.109909	−2.811767	−0.734303
F	−2.994009	−0.465080	−0.499114	F	−2.488122	−0.002353	−0.169151
H	−0.928316	3.151159	0.273214	F	−0.947828	1.121193	−1.249543
H	−3.562010	−1.132651	−0.420859	F	−0.944707	−1.120001	−1.251503

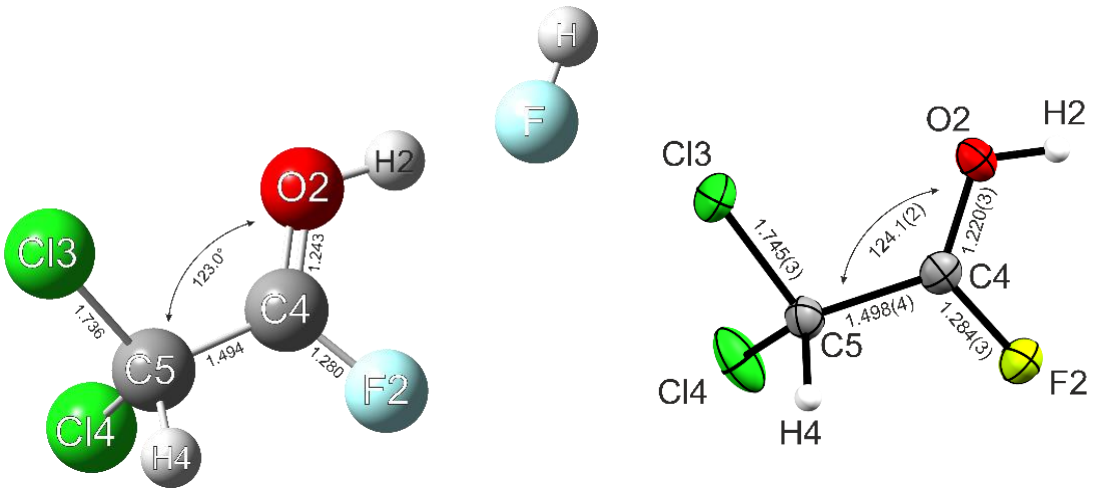

Figure S16. Calculated gas phase structure of $[CClH_2C(OH)F]^+\cdot HF$, $[CH_2FC(OH)F]^+\cdot HF$ and $[CCl_2HC(OH)F]^+\cdot HF$. Bond lengths are given in [Å]. Calculated at the MP2/aug-cc-pVTZ-level of theory.[18]

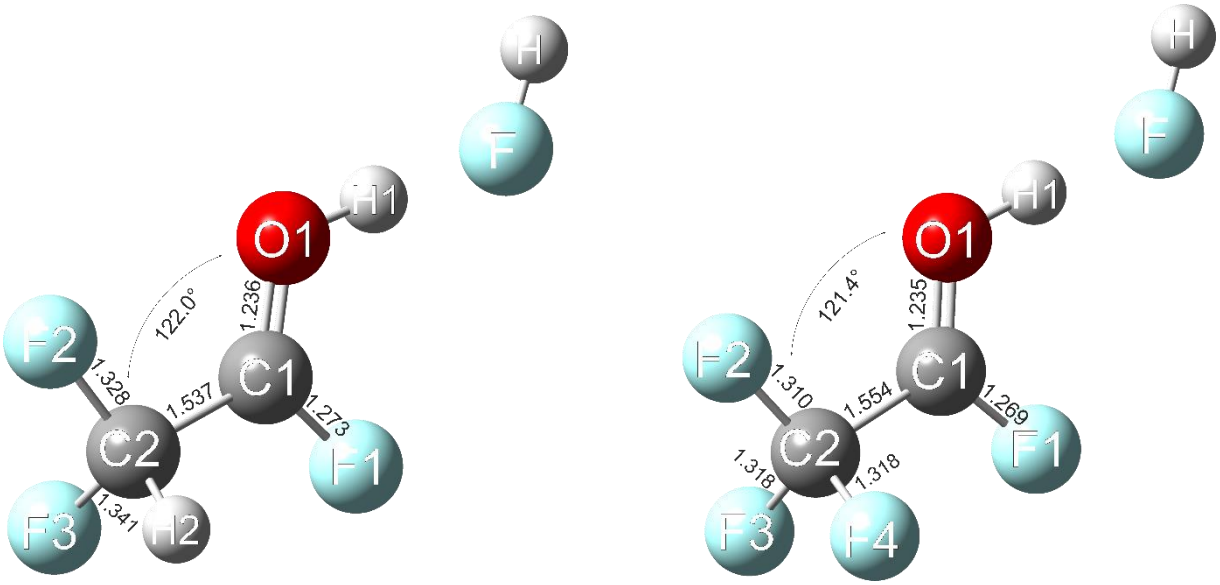

Figure S17. Calculated gas-phase structure of $[CHF_2C(OH)F]^+ \cdot HF$ and $[CF_3C(OH)F]^+ \cdot HF$. Bond lengths are given in [Å]. Calculated at the MP2/aug-cc-pVTZ-level of theory.

Table S9. Standard orientations of CCl_2HCOF. Calculated at the MP2/aug-cc-pVTZ-level of theory.

CCl_2HCOF							
Atom	Coordinates [Å]			Atom	Coordinates [Å]		
	X	Y	Z		X	Y	Z
Cl	−1.076569	−1.445766	0.004091	C	1.224440	−0.026936	−0.099340
Cl	−0.989599	1.498655	0.060117	C	−0.227538	0.012408	−0.539772
F	1.355215	−0.111386	1.218811	H	−0.256977	0.034945	−1.621337
O	2.150436	0.019448	−0.825604				

Table S10. Standard orientations of $[CCl_2HC(OH)F]^+ \cdot HF$. Calculated at the MP2/aug-cc-pVTZ-level of theory.

$[CCl_2HC(OH)F]^+ \cdot HF$							
Atom	Coordinates [Å]			Atom	Coordinates [Å]		
	X	Y	Z		X	Y	Z
F	3.600136	0.210534	−0.392221	C	0.475431	−0.069340	0.404939
Cl	−1.687039	1.470255	0.006152	C	−1.015404	−0.051081	0.503769
Cl	−1.429455	−1.414090	−0.559956	H	−1.319919	−0.299024	1.518026
F	1.096699	−0.904421	1.149372	H	2.113623	0.489556	−0.401840
O	1.111181	0.652636	−0.381464	H	4.265573	0.601075	−0.916416

Table S11. Standard orientations of $[CHF_2C(OH)F]^+ \cdot HF$.

$[CHF_2C(OH)F]^+ \cdot HF$							
ωB97XD/aug-cc-pVTZ				MP2/aug-cc-pVTZ			
Atom	Coordinates [Å]			Atom	Coordinates [Å]		
	X	Y	Z		X	Y	Z
F	−3.235917	−0.135312	−0.166721	F	−3.235917	−0.135312	−0.166721
F	−0.430602	1.374870	0.321046	F	−0.135312	1.374870	0.321046
O	−0.801150	−0.741137	−0.015966	O	−0.801150	−0.741137	−0.015966
C	−0.017095	0.185293	0.188190	C	−0.017095	0.185293	0.188190
C	1.507863	−0.037070	0.302837	C	1.507863	−0.037070	0.302837
H	−1.791800	−0.515106	−0.048259	H	−1.791800	−0.515106	−0.048259
H	−3.950343	−0.684357	−0.395026	H	−3.950343	−0.684357	−0.395026
F	1.759039	−1.314044	0.073035	F	1.759039	−1.314044	0.073035
F	2.058502	0.738782	−0.631847	F	2.058502	0.738782	−0.631847
H	1.847538	0.260554	1.301240	H	1.847538	0.260554	1.301240

Table S12. Standard orientations of $[CF_3C(OH)F]^+ \cdot HF$.

$[CF_3C(OH)F]^+ \cdot HF$							
ωB97XD/aug-cc-pVTZ				MP2/aug-cc-pVTZ			
Atom	Coordinates [Å]			Atom	Coordinates [Å]		
	X	Y	Z		X	Y	Z
F	−3.476771	−0.094824	−0.019155	F	3.484095	0.094923	0.000649
F	−0.618953	1.322108	−0.039932	F	0.608713	−1.373546	−0.000323
O	−1.043765	−0.803385	0.082526	O	1.070268	0.753741	−0.000709
C	−0.217638	0.115413	0.019816	C	0.251220	−0.162336	−0.000301
C	1.262479	−0.111034	−0.027982	C	−1.290007	0.114609	0.000034
H	−2.017940	−0.540605	0.042523	H	2.062588	0.507019	−0.000665
H	−4.235675	−0.629678	−0.022559	H	4.231273	0.648619	−0.001649
F	1.667011	−0.704406	1.115155	F	−1.491742	1.403970	−0.001719
F	1.715415	1.160716	−0.027884	F	−1.778943	−0.444300	1.084096
F	1.639374	−0.842362	−1.098314	F	−1.780262	−0.447626	−1.081636

Table S13. Calculated NPA charges of CCl_2HCOF, CHF_2COF, CF_3COF, $[CCl_2HC(OH)F]^{+}\cdot HF$, $[CHF_2C(OH)F]^{+}\cdot HF$, and $[CF_3C(OH)F]^{+}\cdot HF$. Calculated at the MP2/aug-cc-pVTZ-level of theory.

CCl_2HCOF		**$[CCl_2HC(OH)F]^{+}\cdot HF$**	
Atom	NPA charge	Atom	NPA charge
		F1	−0.563
Cl1	0.005	Cl2	0.099
Cl2	0.005	Cl3	0.082
F3	−0.377	F4	−0.289
O4	−0.584	O5	−0.618
C5	0.991	C6	1.155
C6	−0.264	C7	−0.317
H7	0.223	H8	0.259
		H9	0.577
		H10	0.615
CHF_2COF		**$[CHF_2C(OH)F]^{+}\cdot HF$**	
Atom	NPA charge	Atom	NPA charge
		F	−0.559
F	−0.370	F	−0.270
O	−0.578	O	−0.602
C	0.948	C	1.107
C	0.604	C	0.606
		H	0.580
		H	0.619
F	−0.372	F	−0.327
F	−0.372	F	−0.333
H	0.139	H	0.180
CF_3COF		**$[CF_3C(OH)F]^{+}\cdot HF$**	
Atom	NPA charge	Atom	NPA charge
		F1	−0.557
F1	−0.365	F2	−0.267
O2	−0.549	O3	−0.597
C3	0.921	C4	1.089
C4	1.043	C5	1.067
		H6	0.582
		H7	0.621
F7	−0.343	F8	−0.309
F6	−0.354	F9	−0.315
F5	−0.354	F10	−0.315

Table S14. Selected energies of donor-acceptor interactions from second-order perturbation theory analysis of CCl_2HCOF, CHF_2COF, CF_3COF, $[CCl_2HC(OH)F]^+\cdot HF$, $[CHF_2C(OH)F]^+\cdot HF$, and $[CF_3C(OH)F]^+\cdot HF$. Calculated at the MP2/aug-cc-pVTZ-level of theory.

	Donor NBO	**Acceptor NBO**	**Stabilizing energy [kJ/mol]**
CCl_2HCOF	LP(F1)	π*(C1–O1)	167.7
CHF_2COF	LP(F1)	π*(C1–O1)	173.0
CF_3COF	LP(F1)	π*(C1–O1)	172.0
$[CCl_2HC(OH)F]^+\cdot HF$	LP(F2)	π*(C4–O2)	270.4
$[CHF_2C(OH)F]^+\cdot HF$	LP(F1)	π*(C1–O1)	283.7
$[CF_3C(OH)F]^+\cdot HF$	LP(F1)	π*(C1–O1)	296.4

Table S15. Calculated MEP values at the π-holes of CCl_2HCOF, CHF_2COF, CF_3COF, $[CCl_2HC(OH)F]^+\cdot HF$, $[CHF_2C(OH)F]^+\cdot HF$, and $[CF_3C(OH)F]^+\cdot HF$. Calculated at the MP2/aug-cc-pVTZ-level of theory.

	π-hole [kJ/mol]
CCl_2HCOF	73.2
CHF_2COF	113.9
CF_3COF	140.8
$[CCl_2HC(OH)F]^+\cdot HF$	633.1
$[CHF_2C(OH)F]^+\cdot HF$	679.8
$[CF_3C(OH)F]^+\cdot HF$	654.8

Hirshfeld Surface Analysis

Hirshfeld surface analysis was performed with the CrystalExplorer software.[11,12] The Hirshfeld fingerprint plots of the cation of **1** are depicted in Figure S18. The different contacts and their percentages of all contacts are noted in the diagrams.

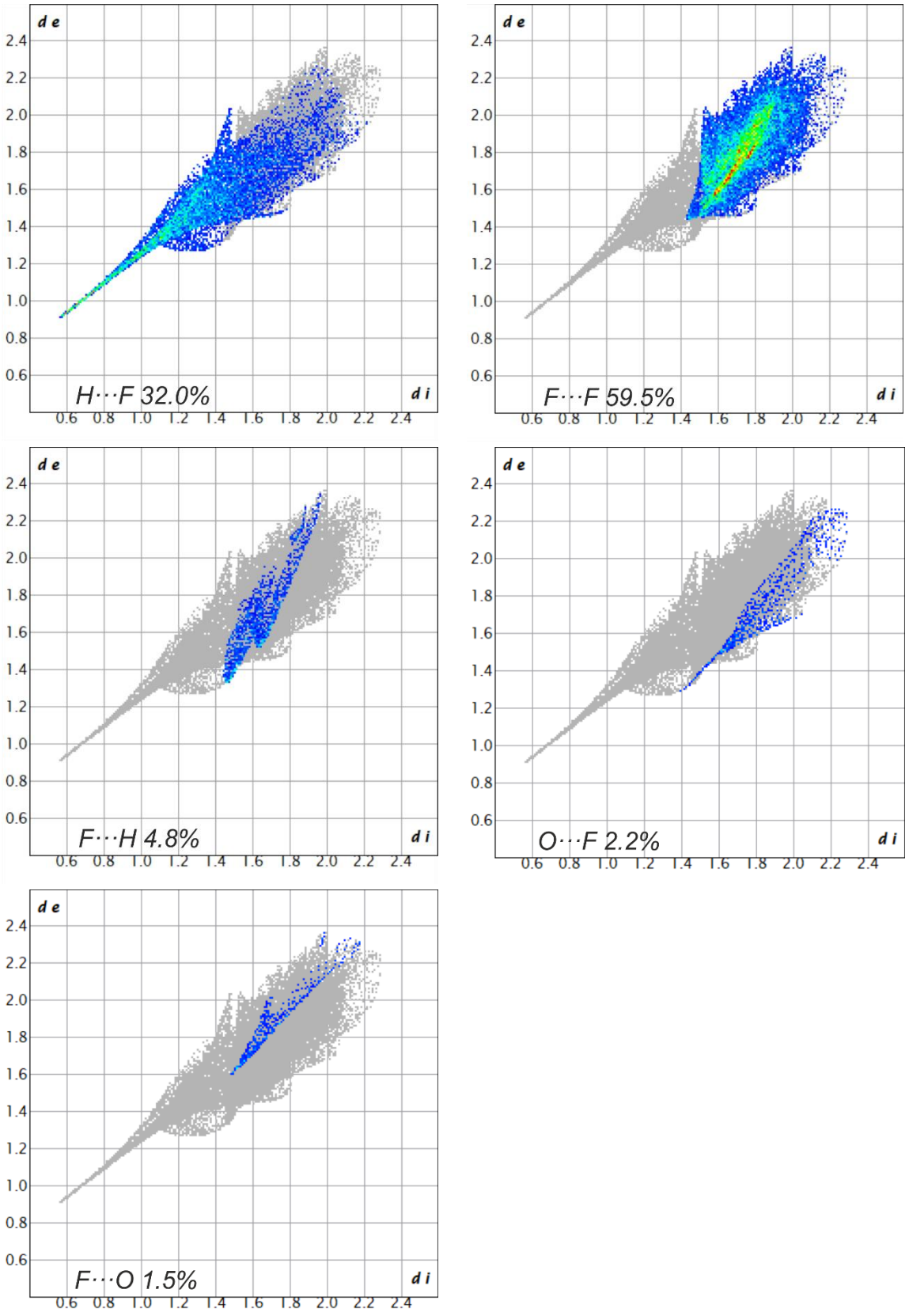

Figure S18. Fingerprint plots of the cation in the crystal structure of **1**.

References

[1] L. Bayersdorfer, R. Minkwitz and J. Jander, *Z. Anorg. Allg. Chem.* 1972, **393**(2), 137.

[2] Rigaku Oxford Diffraction, CrysAlisPro Software System, *Version 1.171.40.82a*, Rigaku Corporation, Oxford, UK, 2020.

[3] G. M. Sheldrick, *Acta Crystallogr. A Found. Adv.* 2015, **71**, 3.

[4] G. M. Sheldrick, *Acta Crystallogr. C Struct.* 2015, **71**, 3.

[5] L. J. Farrugia, *Journal of Applied Crystallography* 1999, **32**(4), 837.

[6] A. Spek, PLATON, *A Multipurpose Crystallographic Tool*, Utrecht University, Utrecht (The Netherlands), 1999.

[7] *SCALE3 ABSPACK – An Oxford Diffraction Program*, Oxford Diffraction Ltd., UK, 2005.

[8] *MestReNova 14.0*, Mestrelab Research, 2019.

[9] M. J. Frisch, G. W. Trucks, H. B. Schlegel, G. E. Scuseria, M. A. Robb, J. R. Cheeseman, G. Scalmani, V. Barone, B. Mennucci, G. A. Petersson, H. Nakatsuji, M. Caricato, X. Li, H. P. Hratchian, A. F. Izmaylov, J. Bloino, G. Zheng, J. L. Sonnenberg, M. Hada, M. Ehara, K. Toyota, R. Fukuda, J. Hasegawa, M. Ishida, T. Nakajima, Y. Honda, O. Kitao, H. Nakai, T. Vreven, J. A. Montgomery, J. E. Peralta, F. Ogliaro, M. Bearpark, J. J. Heyd, E. Brothers, K. N. Kudin, V. N. Staroverov, R. Kobayashi, J. Normand, K. Raghavachari, A. Rendell, J. C. Burant, S. S. Iyengar, J. Tomasi, M. Cossi, N. Rega, J. M. Millam, M. Klene, J. E. Klene, J. E. Know, J. B. Cross, V. Bakken, C. Adamo, J. Jaramillo, R. Gomperts, R. E. Stratmann, O. Yazyev, A. J. Austin, R. Cammi, C. Pomelli, J. O. Ochterski, R. L. Martin, K. Morokuma, V. G. Zakrzweski, G. A. Voth, P. Salvador, J. J. Dannenberg, S. Dapprich, A. D. Daniels, O. Farkas, J. B. Foresman, J. V. Ortiz, J. Cioslowski and D. J. Fox, *Gaussian16, Revision C.01*, Gaussian Inc., Wallingford CT, 2016.

[10] R. Dennington, T. A. Keith and J. M. Millam, *GaussView Version 6.0*, Semi-chem Inc. Shawnee Mission, KS, 2016.

[11] S. K. Wolff, D. J. Grimwood, J. J. McKinnon, M. J. Turner, D. Jayatilaka and M. A. Spackman, *CrystalExplorer 17.5, Revision: f4e298a*, University of Western Australia, 2017.

[12] M. A. Spackman and D. Jayatilaka, *CrystEngComm* 2009, **11**, 19.

[13] J. R. Durig, G. A. Guirgis and T. A. Mohamed, *J. Mol. Struct.* 1998, **444**, 165

[14] G. D. Bent, E. Zerrad, G. W. Trucks, K. B. Wiberg and L. Taing, *J. Phys. Chem. A* 2000, **104**, 370.

[15] G. M. Sheldrick, *Acta crystallographica. Section A, Foundations and advances* 2015, **71**, 3.

[16] G. M. Sheldrick, *Acta crystallographica. Section C, Structural chemistry* 2015, **71**, 3.

[17] A. F. Baxter, J. Schaab, J. Hegge, T. Saal, M. Vasiliu, D. A. Dixon, R. Haiges and K. O. Christe, *Chem. Eur. J.* 2018, **24**, 16737

[18] S. Steiner, A. Nitzer, C. Jessen and A. J. Kornath, *Z. Anorg. Allg. Chem.* 2024, **650**, e2024000136.